3-2008

Design of an Oxygen Turbopump for a Dual Expander Cycle Rocket Engine

William S. Strain

DESIGN OF AN OXYGEN TURBOPUMP FOR A DUAL EXPANDER CYCLE ROCKET ENGINE

THESIS

William S. Strain, Captain, USAF

AFIT/GAE/ENY/08-M26

DEPARTMENT OF THE AIR FORCE
AIR UNIVERSITY
AIR FORCE INSTITUTE OF TECHNOLOGY
Wright-Patterson Air Force Base, Ohio

The views expressed in this thesis are those of the author and do not reflect the official policy or position of the United States Air Force, Department of Defense, or the U.S. Government.

AFIT/GAE/ENY/08-M26

DESIGN OF AN OXYGEN TURBOPUMP FOR A DUAL EXPANDER CYCLE ROCKET ENGINE

THESIS

Presented to the Faculty

Department of Aeronautics and Astronautics

Graduate School of Engineering and Management

Air Force Institute of Technology

Air University

Air Education and Training Command

In Partial Fulfillment of the Requirements for the

Degree of Master of Science in Aeronautical Engineering

William S. Strain, BS

Captain, USAF

March 2008

AFIT/GAE/ENY/08-M26

DESIGN OF AN OXYGEN TURBOPUMP FOR A DUAL EXPANDER CYCLE ROCKET ENGINE

William S. Strain, BS

Captain, USAF

Approved:

_____	_____
Richard D. Brannam, Maj, USAF (Chairman)	Date
_____	_____
Robert B. Greendyke (Member)	Date
_____	_____
Paul I. King (Member)	Date

Acknowledgments

I would like to express my sincere appreciation to my faculty advisor, Maj Richard Branam, for his guidance and support throughout the course of this thesis effort. The insight, experience and help was greatly appreciated. I would also like to thank Capt Michael Arguello for his help with aesthetic issues and for serving as a sounding board during the design process.

I would also like to thank my grandfather for the love and support he gave me during his life, and the work ethic and persistence he instilled in me. My thanks also go to Dr. Elias C. Mattas whose design class taught me how to think through the design process, be it for a refinery or a rocket engine, and whose kind recommendation played no small role in my acceptance to OTS. My sincerest thanks and deep gratitude also to Dr. Perwaiz Meraj, M.D. whose support was vital during a very difficult time in my life and whose friendship has made me happier and healthier for over a decade.

William S. Strain

Table of Contents

Page

List of Figures

Page

List of Tables

Page

Nomenclature

Acronyms	Description
DEAN	Dual Expander Aerospike Nozzle
EELV	Evolved Expendable Launch Vehicle
IHPRPT	Integrated High Payoff Rocket Propulsion Technology
I_{sp}	Specific Impulse (s)
JAXA	Japanese Aerospace Exploration Agency
LOX	Liquid Oxygen
NIST	National Institute of Standards and Technology
NPSH	Net Positive Suction Head
NPSS	Numerical Propulsion Simulation System

Symbols	Description
A	Area (ft^2 or m^2)
AR	Area Ratio
B	Blockage
C	Absolute Flow Velocity (ft/s or m/s) or Blade Cord (Eq. 49) (in or cm)
c^*	Characteristic Velocity (ft/s or m/s)
DR	Diffusion Ratio
g_o	acceleration due to gravity at sea level (ft/s^2 or m/s^2)

h	Specific Enthalpy (ft^2/ s^2 or m^2/s^2)
H	Head (ft or m)
I	Incidence (degrees)
LC	Loss Coefficient
N	Rotational Speed (RPM)
P	Pressure (psi or Pa) or Power (hp or kW) (Chap.3)
Q	Volumetric Flow Rate (ft^3/ s or m^3/s)
R	Radius (in or cm) or exhaust gas constant (eq. C)
s	Specific Entropy
U	Blade Tip Speed (ft/s or m/s)
W	Relative Velocity (ft/s or m/s)
Z	Blade Number
$\dot{m}$	Mass Flow Rate (lbm/s or kg/s)

Greek Symbols

ε	Secondary Area Ratio; exit clearance; nozzle expansion ratio
χ	Secondary Mass Fraction
ρ	Density (lbm/ft^3 or kg/ m^3)
α	Flow Angle (degrees)
ψ	Loading Coefficient
φ	Flow Coefficient
β	Relative Flow Angle (degrees); Subscript b Denotes Blade Angle
σ	Slip Factor
ξ	Meridional Velocity Ratio
η	Efficiency
γ	Heat capacity ratio
λ	Nozzle efficiency; inlet swirl parameter

Station Numbering

Pump

0	Up Stream/ Stage Inlet
1	Impeller Inlet
2	Impeller Exit
5	Diffuser Exit
7	Volute Throat

8	Stage Exit

Turbine

4	Rotor Inlet
6	Rotor Exit

Subscripts

0	Denotes Total Conditions
c	Combustion
e	Exit
i	Inlet
m	Meridional
p	pump
t	Tangential
T	Turbine

Abstract

The design of a pump intended for use with a dual expander cycle (LOX/H_2) engine is presented. This arrangement offers a number of advantages over hydrogen expander cycles; among these are the elimination of gearboxes and inter-propellant purges and seals, an extended throttling range, and higher engine operating pressures and performance. The target engine has been designed to meet the needs of Phase III of the Integrated High Payoff Rocket Propulsion Technology (IHPRPT) program; thus, this pump must meet the program's reliability, maintainability, and service life goals. In addition, this pump will be driven by warm gaseous oxygen. In order to meet the needs of this engine, the pump will need to be capable of delivering 106 lbm/s (48.1 kg/s) at 4500 psi (31 MPa); this will necessitate a turbine capable of supplying at least 2215 hp (1652 kW). The pump and turbine were designed with the aid of an industry standard design program; the design methodology and justification for design choices are presented. Appropriate materials of construction and bearings for this pump are discussed.

CONCEPTUAL DESIGN OF AN OXYGEN PUMP FOR USE IN A DUAL-EXPANDER CYCLE ENGINE

1 Introduction

1.1 Motivation

The Integrated High-Payoff Rocket Propulsion Technology (IHPRPT) program was initiated in 1994 with the goal of doubling US rocket propulsion capabilities by 2010 (as measured against the 1993 baseline). The goals are summarized in Table 1, taken from Blair and DeGeorge.[1] The main goals of interest are increased payload (which this effort will accomplish by increasing I_{sp} of the upper stage), cost reduction[2] and reliability improvement. Additionally, as this program envisions the use of a reusable launch vehicle[3], the ability to perform aircraft-like operations and thus reliability and maintainability is highly valued.

The Centaur upper stage used on both EELV variants (the Delta IV and Atlas V) is powered by the RL-10 engine, described in detail in section 2. The heavy variants of these launch systems are capable of boosting payloads of 21,890 kg to LEO and 6,280 kg to GEO.[4] When compared to foreign counterparts, the US appears to be falling behind in its technological advantage. The H-IIA, operated by the Japanese Aerospace Exploration Agency (JAXA), utilizes an LE-5B upper stage engine.[5] This vehicle has a LEO (300 km, circular 30° orbit) payload capability of 10,000 kg (22,000 lb). The Ariane 5 ESC-B upper stage powered by the Vinci engine has payload capacity of 12,000 kg (26,400 lb) to geostationary transfer orbit.[6]

Table 1: IHPRPT Goals for boost and orbit transfer[1]

Boost and Orbit Transfer Propulsion	**Phase I**	**Phase II**	**Phase III**
Reduce Stage Failure Rate	25%	50%	75%
Improve Mass Fraction (Solids)	15%	25%	35%
Improve I_{sp} (Solids)	2%	4%	8%
Improve I_{sp} (sec) (Liquids)	14	21	26
Reduce Hardware Cost	15%	25%	35%
Reduce Support Costs	15%	25%	35%
Improve Thrust to Weight (Liquids)	30%	60%	100%
Mean Time Between Removal (Mission Life: Reusable)	20	40	100

In support of the IHPRPT goals, a study was performed at AFIT to examine the design of a dual expander cycle upper stage LOX/H_2 engine with an aerospike nozzle to accomplish IHPRPT Phase III goals. The LOX/H_2 combination was chosen because of its potential to achieve high I_{sp} values relative to other liquid propellant systems such as LOX/RP. Maximizing I_{sp} in an upper stage has a greater positive effect on payload capacity than doing likewise in a first stage.[7] This engine, shown schematically in Figure 1, was designed with a target I_{sp} of 464 s and a thrust goal of 50,000 lb_f (222 kN). In the phase III concept engine, LOX will be used to cool the chamber wall while H_2 is used to cool the nozzle and aerospike. Each propellant is to have its own pump and turbine driven by heat pickup from the respective cooling circuits. This arrangement negates the need for a gearbox required for single-turbine engines such as the one employed on the current upper stage engine, the Pratt & Whitney RL-10.[8] Avoiding the use of a gearbox will result in lower weight and greater operability for the dual expander concept. Additionally, this approach will eliminate the inter-propellant seal and purge fluid systems necessary in a hydrogen-only expander cycle. The elimination of this seal eliminates the critical failure possibility; however, it will also require hot oxygen tolerant

turbine materials.[9]

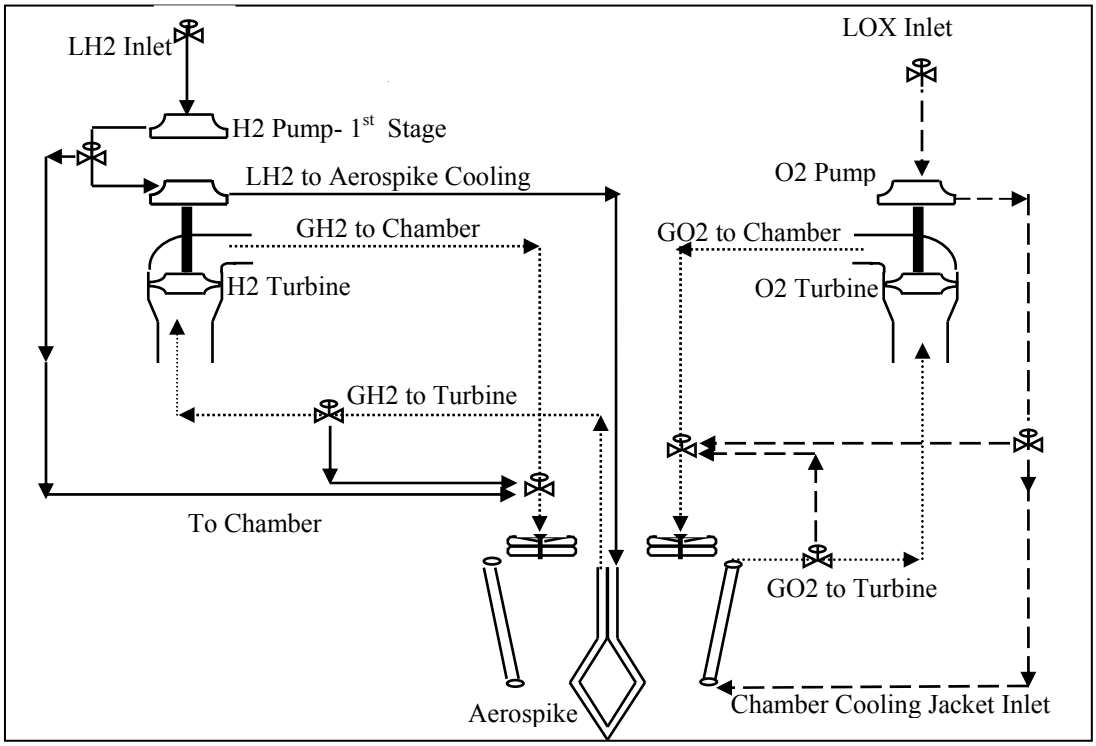

Figure 1: Dual Expander Cycle engine schematic

Further, a dual expander cycle is better suited to the high cycle life, mean time between removal, and throttleability targets since the heat pickup demands on the hydrogen circuit are less than for a comparable hydrogen expander cycle.[10] The elimination of the inter-propellant seals and purges also facilitates the reliability goal when many restarts will be required. In comparison to other rocket cycles, an expander cycle engine is also inherently safer, as it avoids the use of multiple combustion chambers. Finally as mentioned by Buckmann, et al., this cycle delivers the propellants to the combustion chamber as superheated gases, resulting in an injector pressure drop which varies

approximately as mass flow instead of mass flow squared.[10] This feature will help maintain stable chamber conditions when the engine is throttled.

1.2 Problem Statement

In order to continue to meet the nation's space lift goals, the Air Force must improve its orbital transfer vehicle capabilities, which necessitates improvements in upper-stage engines; this need is the driving force behind the IHPRPT program. The Dual Expander Aerospike Nozzle (DEAN) engine has been designed to meet the 2010 goals set out in the Phase III IHPRPT program.[1] This engine concept will require an oxygen pump capable of supporting the program's reliability, maintainability, and service life goals while delivering the required flow at the required pressure. Additionally, this pump must be powered by (and thus be resistant to) hot oxygen and have the ability to operate stably over a range of flow rates.

1.3 Research Goals

This effort details the design of an oxygen turbopump required by a dual expander cycle upper stage engine intended to meet the Phase III IHPRPT requirements. The primary objectives of this effort are fourfold:

1. to deliver LOX flow at the operating conditions required by this engine
2. to include design features supporting reliability goals of the IHPRPT Phase III requirements
3. to analyze throttling capability over a range of flow rates

4. to ensure the pump concept can support aircraft-like operations, is maintainable and reusable with acceptable service life.

1.4 Research Focus

This work focuses on the design of the impeller and turbine necessary for this pump. Of most interest is the design of the components, especially the turbine rotor and pump impeller necessary for this pump to achieve the performance, maintainability, and reliability goals set out by the Phase III IHPRPT program. Further, the components must be capable of supporting throttled operation, thus off-design performance will be important. Finally, this work will explore the materials and bearings required for the pump to be successful.

2 Literature Review

This chapter starts with a survey of current and planned LOX/H_2 upper-stage engines and their LOX pumps. It concludes with an exploration of details of design features critical to pump success and the attainment of the objectives set out in Chapter 1.

2.1 Current Systems

Due to unique advantages of LOX/H_2 upper-stage engines, such as greater I_{sp}, there are a number in use today. These include the RL-10 which powers the Centaur upper stage on both EELV variants, the LE-5 used by the Japanese Aerospace Exploration Agency (JAXA), and the Vinci used by the European Space Agency (ESA). This section will discuss these with special attention paid to their LOX pumps, and conclude with an Aerojet effort which developed a LOX pump intended for an upper stage application.

2.1.1 Pratt & Whitney RL10

The RL-10 is used on the Centaur and has a long track record as a reliable engine having been originally developed in the 1960s, and it was the first flight engine to have bearings lubricated and cooled by liquid hydrogen.[11,12] As shown in Figure 2, it relies on a hydrogen expander cycle to power the turbine and a geared arrangement to drive both the LOX and H_2 pumps.[13] The RL10-A4's LOX pump delivers 17.78 kg/s (39.1 lb/s) at 5,725 kPa (830.6 psi) with a design speed of 14300 rpm. As noted by Brannam, et al[14], the hydrogen expander cycle used by this engine is capable of only modest improvements over the baseline RL-10A-3-3A. This engine's growth potential is limited due to power extraction requirements from the cooling circuit.

The hydrogen must be heated to temperatures near the design limit for alloys currently used in the chamber liner.

Other limits of this engine cycle that make it an unattractive candidate for this application include:

1. While the RL-10 is designed to have restart capability, it is designed for a relatively short life.
2. The RL-10 has a high parts count, a large gearbox vital to its operation, and requires many hours of touch labor, suggesting that it would be difficult to achieve the IHPRPT maintainability goal with this type of engine configuration.
3. A single expander cycle is capable of only a limited throttling range. When other IHPRPT goals such as mean time between removal, the ability to have multiple starts, and throttleability are considered, the limitations of this cycle make it a less than ideal candidate for this application.

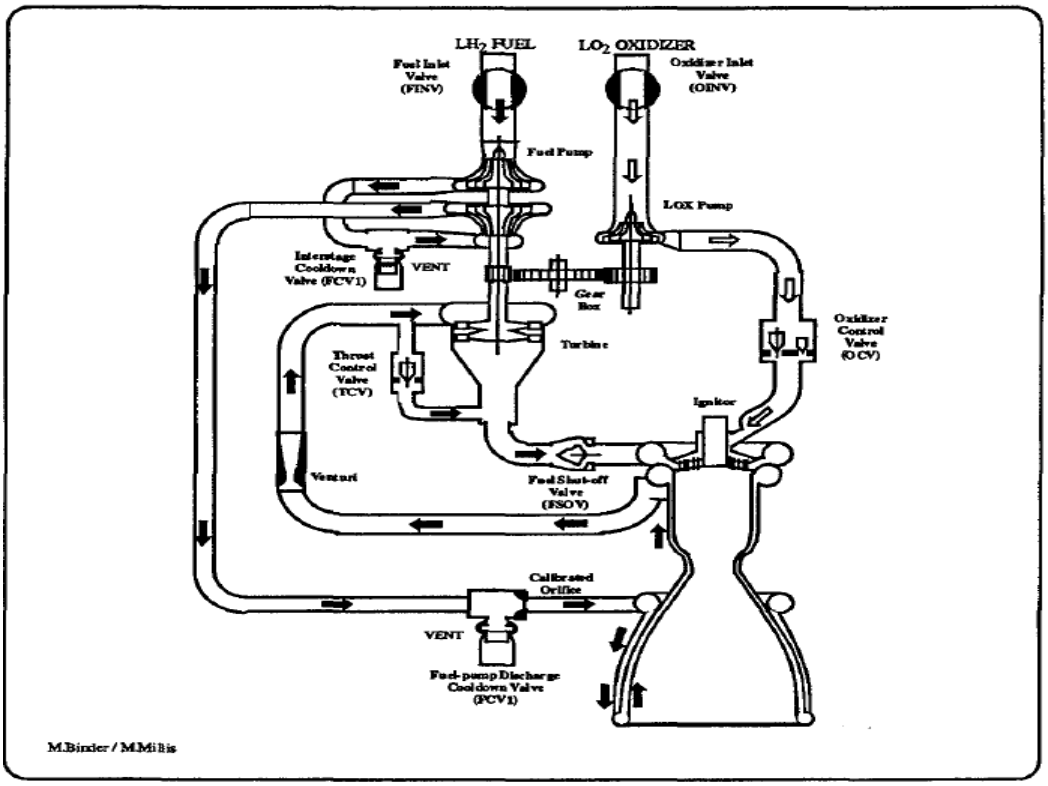

Figure 2: RL-10 Schematic[13]

2.1.2 LE-5B

The LE-5 is used on the upper stage of the Japanese H-II rocket.[15] It uses a single expander cycle to power both LOX and H_2 pumps with H_2 as the drive gas for both turbines, and is designed to deliver 137 kN (30,800 lb) of thrust with a specific impulse of 448 s. Its attributes are summarized in Table 2. Its LOX pump delivers 19.4 kg/s (42.7 lb/s) at a design speed of 17,000 rpm. Throttling and the ability to have multiple burns with long coast phases were two design priorities during the development of this engine. It is expensive compared to other similar engines.[15] Like the Vinci engine (below), it requires an inter-propellant seal and purge system for the oxygen turbopump.

Table 2: LE-5B Performance Characteristics[15]

	LE-5B	LE-5A
Thrust (in Vacuum) [kN]	137	122
Isp (in vacuum) [sec]	450	453
Engine Mixture Ratio	5	5
Chamber Pressure [MPa]	3.6	4.0
FTP Rotational Speed [rpm]	50200	50500
LTP Rotational Speed [rpm]	17100	17400
Turbine Inlet Temperature [K]	380	600

2.1.3 Vinci

The Vinci is the upper stage of the Ariane 5. It has a design thrust of 180 kN (40,000 lb)[16], a design I_{sp} of 464 s and uses an expander cycle, as shown in Figure 3. Similar to the LE-5B, H_2 is the drive gas for both turbines. It is intended to be capable of five restarts. While the dual-turbine design eliminates the need for a gearbox (as in the RL-10), it requires an inter-propellant seal and associated purge system for the oxygen turbopump, which will add weight and negatively impact reliability and maintainability. Thus, this engine cycle is not the ideal candidate for IHPRPT Phase III application.

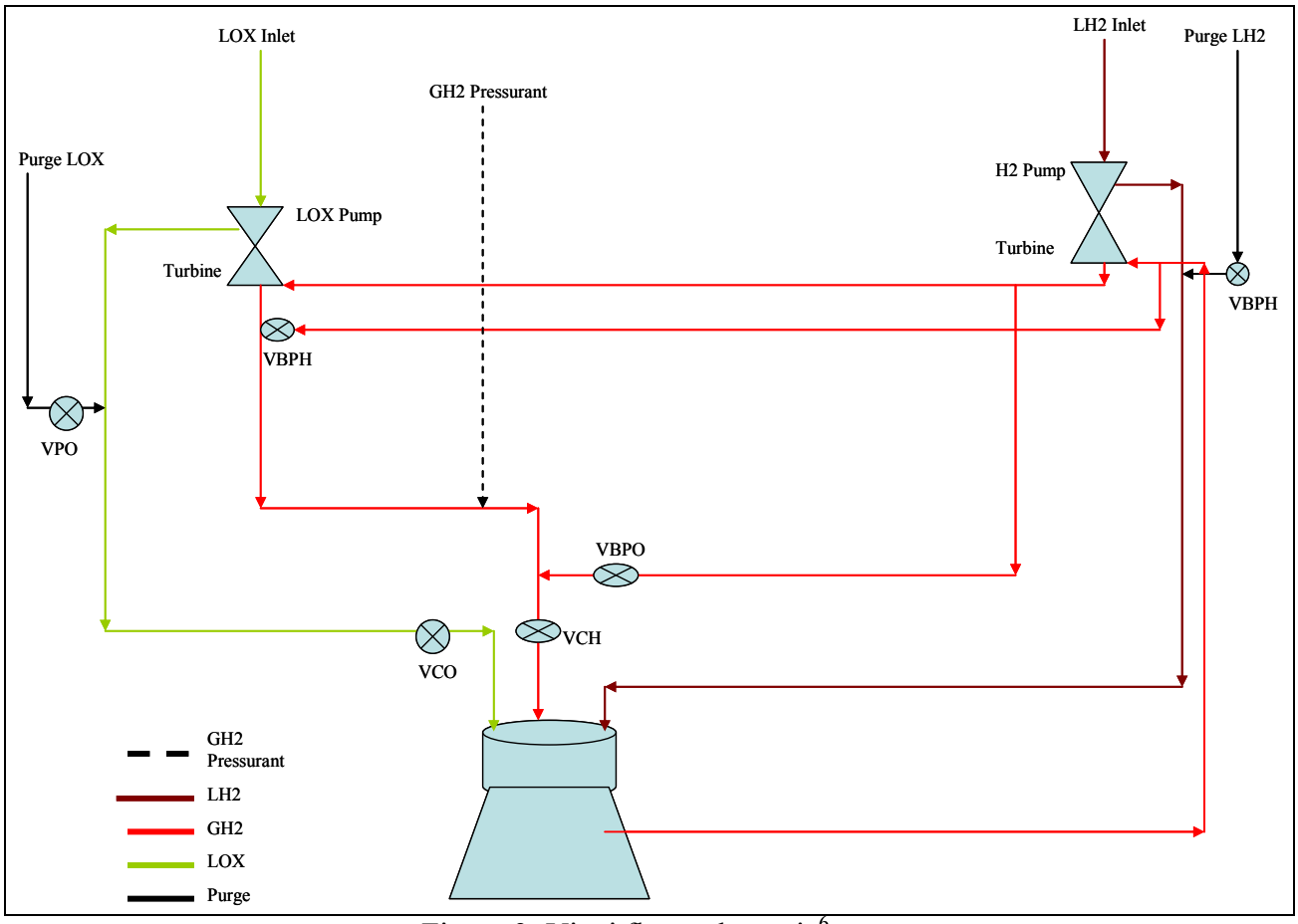

Figure 3: Vinci flow schematic[6]

2.1.4 Aerojet Orbital Transfer Vehicle Engine

Beginning in July of 1983, Aerojet designed and built an oxygen turbopump intended for use in a dual expander cycle engine on an orbital transfer vehicle.[9,10,,17] This engine is shown schematically in Figure 4 and, unlike the target engine considered in this work, this engine does not use an aerospike nozzle. Additionally, this engine will require an H2/O2 heat exchanger that the DEAN will not. As a result, this engine does not offer the potential weight savings of the DEAN. This engine design produces 3,750 lb_f of thrust; design parameters for the oxygen pump are shown in Tables 3 and 4. This pump was designed with a two-stage impeller and a single

stage, full admission turbine. A boost pump was required, driven by a hydraulic turbine supplied by a tap-off from the inducer discharge. The rolling element bearings have reliability issues and life limitations due to the high operating speed (75,000 rpm).[7] To avoid these problems, LOX-lubricated hydrostatic bearings were deemed necessary to meet the service life goals (500 starts/20 hours between overhauls and 100 starts/4hours with no service necessary[17]). This pump was tested at speeds up to 69,800 rpm (93% of design speed) for a total run time of 37 minutes while driven by nitrogen. The pump achieved 88% of its design discharge pressure when driven with ambient temperature oxygen. The bearings operated successfully, with no abnormal wear. However, hot oxygen testing was not performed[17].

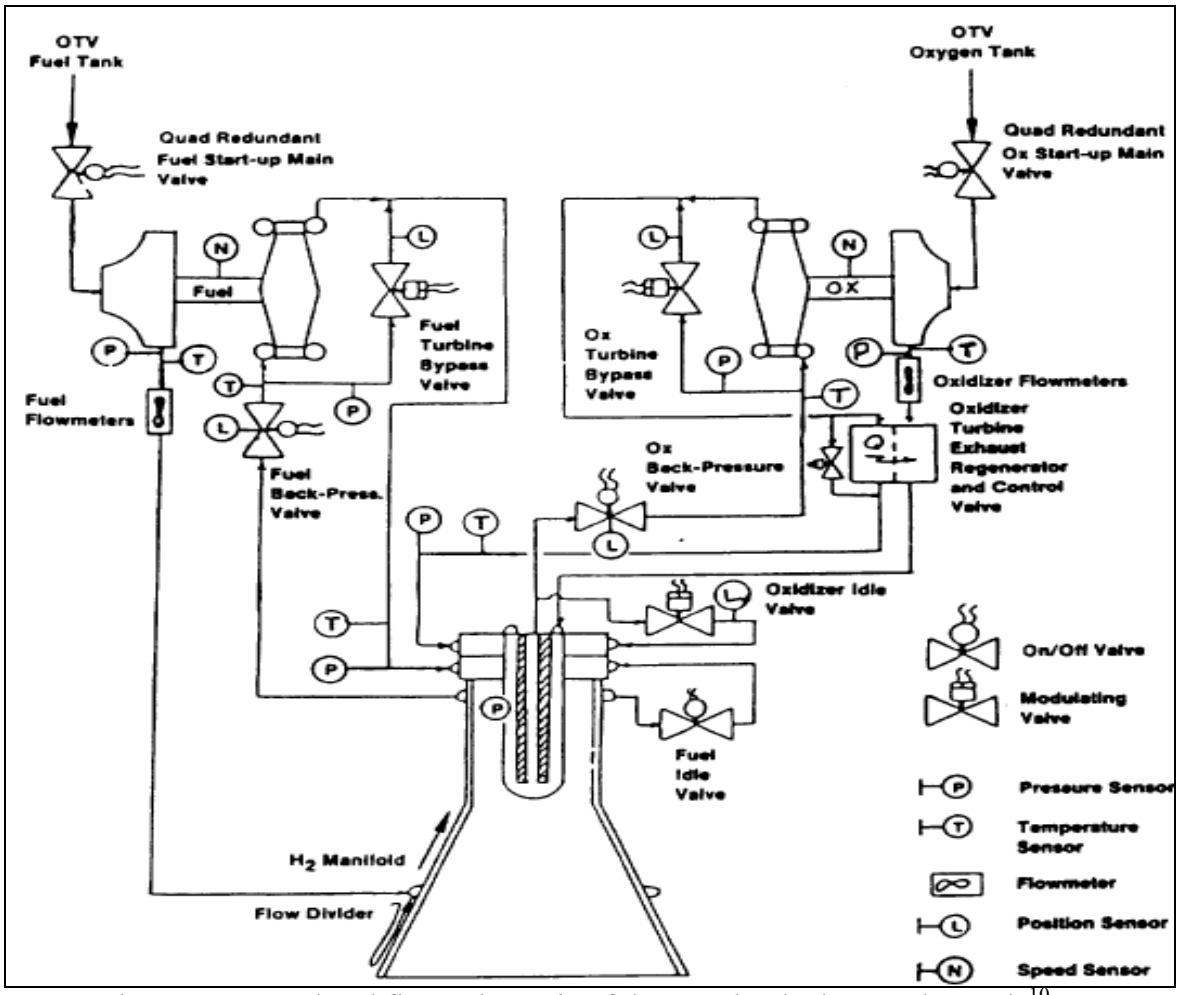

Figure 4: Control and flow schematic of the Aerojet dual expander cycle[10]

Table 3: Aerojet LOX pump design point[9]

	Boost Pump	High Pressure Pump
Number of Stages	1	2
Weight Flow, lb/sec	5.5	5.5
Volume Flowrate- Inducer, gpm	-	51.4
Volume Flowrate- Impellers, gpm	34.7	34.7
Suction Pressure- psia	15.0	54.6
Discharge Pressure- psia	54.6	4654.6
Inducer Head Rise- ft	-	525
Head Rise per Stage- ft	80	4575
Speed, rpm	12,700	75,000
Stage Specific Speed, US units	2,722	787
Impeller Discharge Diameter- in	1.41	1.62
Impeller Discharge Port Width- in	0.097	.0812
Efficiency, %	65.0	59.0
Net Positive Suction Head, ft	0 (TSH = 4.3 ft)	80
Suction Specific Speed,	24,800	20,100
*TSH- Thermodynamic Suppression Head		

Table 4: Aerojet LOX pump design point parameters[9]

Pump	LOX
Weight Flow- lb/sec	5.5
Volume Flow- gpm	34.7
Pressure Rise- psi	4600
Speed- rpm	75000
Efficiency- %	59
Specific Speed, rpm, gpm ,ft	790
Turbine	GOX
Weight Flow- lb/sec	5.1
Inlet Temperature, ^{o}R	860
Inlet Total Pressure- psia	4315
Outlet Static Pressure- psia	2236
Efficiency (total-to static)- %	67
Horsepower- shp	156

2.2 Technical Issues

In order for a LOX pump to successfully fulfill the goals laid out in Chapter 1, a number of technical hurdles must be addressed. First, materials must be found that can tolerate both LOX (inducer and impeller) and hot oxygen (turbine). Bearings must be selected satisfying the reliability and service life goals. The impeller and diffuser must be designed in such a way as to maximize throttleability. Finally, sound design methods must be used to complete the hydraulic design of the inducer, impeller, and turbine.

2.2.1 Materials

Past LOX pumps intended for use on expendable platforms have successfully used impellers and casings fashioned from such materials as cast aluminum, stainless steel, Inconel 718, and K Monel.[18,19,20] The use of the first two materials poses a fire risk due to a lack of ignition resistance in the event of a material rub. The casing on the LOX turbopump used in the Vulcain engine was changed from aluminum to Inconel after such a fire in the early 1990s.[21] Turbine materials for such applications (which used LOX/RP-1 or LOX/H_2 combustion products as the drive gas) included Stellite 21, Hastelloy B and C, and Inconel 718.[22] In contrast, this pump will use high-pressure, high velocity oxygen as the turbine drive fluid. It is thus very important from both a safety and reliability standpoint to ensure the turbine is fabricated from a material tolerant to this expected environment without experiencing damage and meeting service life goals.

Likewise, the impeller material must be resistant to the potential hazards of rubbing friction and foreign particle damage in a liquid oxygen environment.[23] The ignition potential from a particle strike or metal rub in pure oxygen was identified by Brannam et al. as the main technology issue in the development of the Aerojet pump.[14]

To assess the suitability of candidate materials for this type of service, Schoenman[24] performed friction rubbing tests and particle impact tests in a high temperature gaseous oxygen environment. Apparatus for these tests are shown schematically in Figures 5 and 6, respectively. A summary of the results of both test results are shown in Table 5. Guided by similar data and the need to have acceptable mechanical properties (qualities lacking in the top three materials in Table 6), Buckmann et al. chose to construct their pump from Monel.[9]

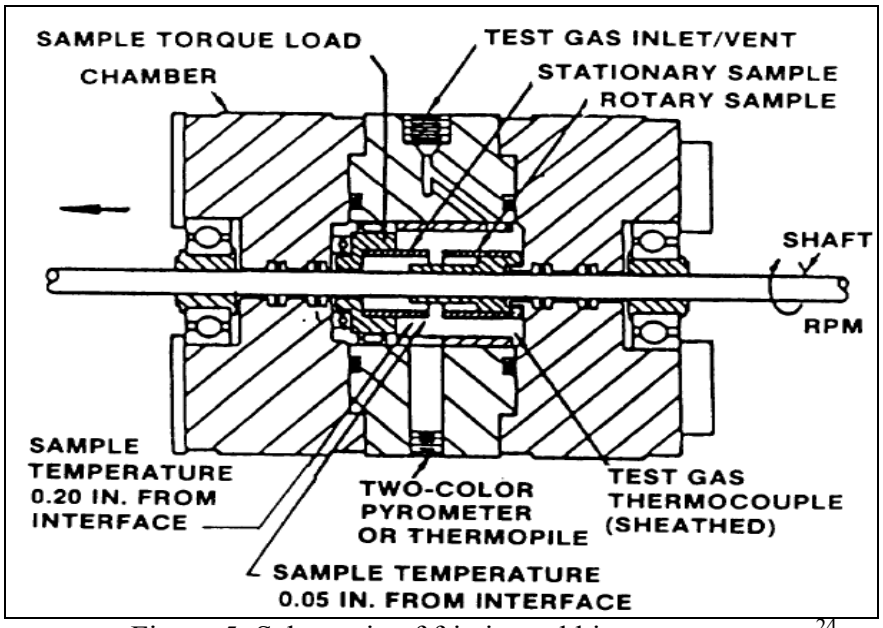

Figure 5: Schematic of friction rubbing test apparatus[24]

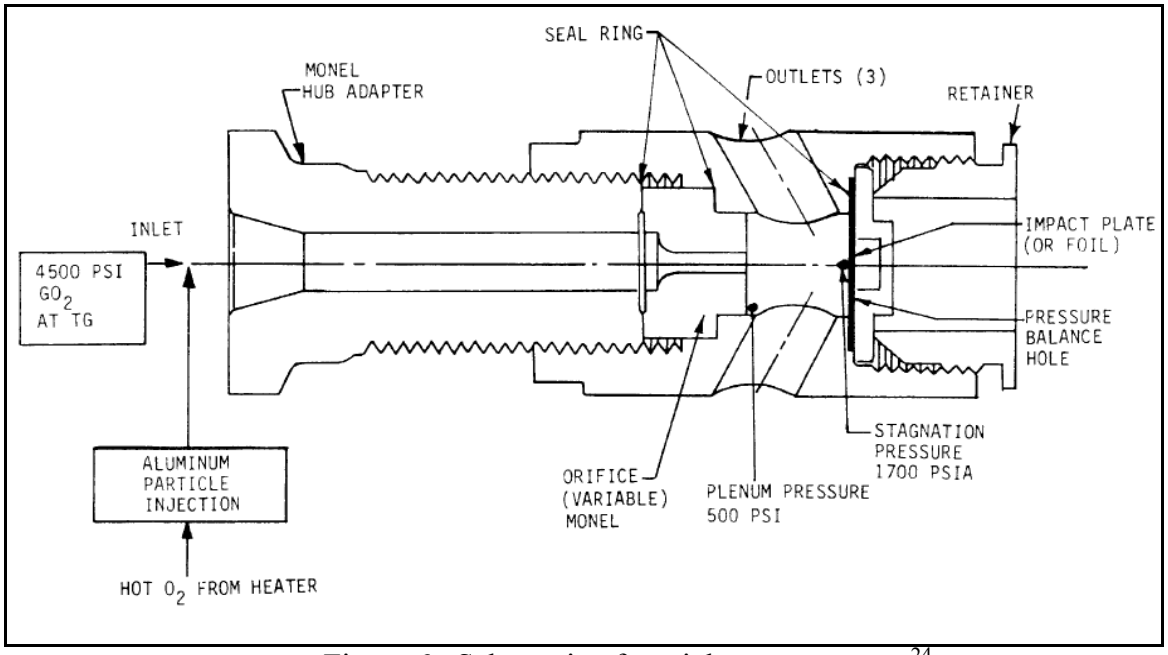

Figure 6: Schematic of particle test apparatus[24]

Table 5: Summary material ignition results[23]

Material	Burn Factor	Observations
Zirconium Copper	35	No ignition in any tests (790/1800°F)
Nickel 200	550	Ignition above 2200°F in FRT only (825/2200°F)
Silicon Carbide	1145	No ignition limited testing (850/ - °F)
Monel 400	1390	Ignition above 1200°F in FRT only (800/1200°F)
K-Monel 500	2090	Ignition above 1500°F in FRT (750/1500°F)
Inconel 600	3226	Ignition above 1100°F in FRT only (- /1000°F)
316 Stainless Steel	4515	Ignition in all tests (450/800°F)
Invar-36	5444	Ignition in all tests (675/340°F)
Hastelloy-X	7160	Ignition in all tests (725/750°F)

2.2.2 Bearings

Bearing inspection and replacement is a time-consuming procedure representing a significant portion of the maintenance cost of a reusable propulsion system[25]. Ball bearing wear has been a recurring life-limiting factor during testing of the Space Shuttle Main Engine[26] and it is believed unlikely their performance will be

bettered by an operational system in the near term. Although Urke suggests an expendable system would not require hydrostatic bearings below a design speed of 40,000 rpm, it is likely a pump whose duty cycle reflects that envisioned by the IHPRPT Phase III requirements will need hydrostatic bearings.[17] Scharrer, Tellier, and Hibbs mentioned several applications where this bearing design choice benefits the overall engine performance, specifically in thrust to weight.[27] By increasing pump speed, the overall weight of the pump can be reduced. An additional benefit of the use of hydrostatic bearings is a reduction in parts count with salutary implications for reliability and maintainability.[28]

2.2.3 Hydraulic Design and Throttleability

The initial performance requirements of the LOX pump considered in this work was obtained by performing a cycle power balance at the design point and using the resulting parameters as inputs into the pump sizing routine suggested in Humble, Henry, and Larson[29]; the resulting pump characteristics are shown in Table 6. There is a wealth of historical practices that apply to the problem of designing an inducer/impeller system to accomplish this task and to the design of a turbine required to drive it.[11,22,30,31] Many of these are based on empirical correlations such as the specific speed/ efficiency chart presented in Urke[17] or the blade number envelope presented in NASA SP-8109.[18]

Oyama and Liou identified the exit blade angle, entrance and exit blade numbers, and blade thickness as design parameters having the most impact on successful impeller design.[32] Veres presents a method for predicting the off-design performance of a centrifugal pump.[33] Off-design performance is of great importance for a pump, as most

pumps are required to operate below design flow for a significant fraction of their service lives.

Veres also presents suggestions for ensuring a pump is capable of a wide throttling range; among these are to specify nearly tangential blade angles, the use of vaneless diffusers, and the use of a higher number of impeller blades.[34]

Based on the need to have a compact, efficient turbopump, a radial inflow turbine design was chosen.[35] Other advantages of this approach as compared to an axial turbine include durability, greater manufacturability, and a higher per-stage work output.[36]

Table 6: Preliminary pump characteristics

Shaft Speed	Rotation/Minute (RPM)	31000
Head Rise	Feet (ft.)	8241.5
Power Required	Brake Horsepower (BHP)	1627.7
Flow	Gallons/Minute (GPM)	591.7
Mass Flow	Pounds Mass/Second (lbm/s)	106.2

3 Methodology

This chapter discusses the design methodology used in this work. It begins with the initial power balance and NPSS results, and proceeds to the impeller and turbine design.

3.1 Initial Power Balance

In order to define the performance parameters required of the pump, an initial power balance was performed using equations below presented in Humble, Henry, and Larson.[29] The master power balance equation is:

$$P_{req} = \frac{g_0 \dot{m} H}{\eta_p} = \eta_t \dot{m} c_p T_i \left[1 - \left(\frac{1}{p_{trat}} \right)^{\frac{\gamma-1}{\gamma}} \right] \tag{1}$$

Where P_{req} represents the required pressure, the quantity to the left of the second equals sign represents the power required by the pump, and the quantity on the right is the power supplied by the turbine; NIST data was used to find the heat capacity and γ at the desired inlet temperature. The turbine expansion ratio, p_{trat}, is simply the ratio of the inlet to outlet turbine pressures, and the outlet turbine pressure is constrained by the combustion chamber pressure. With the goal I_{sp} known, this may be found by using equations (2) through (5) below:

$$I_{sp} = \lambda \left\{ \frac{c^* \gamma}{g_0} \sqrt{\left(\frac{2}{\gamma - 1} \right) \left(\frac{2}{\lambda + 1} \right)^{\frac{\gamma+1}{\gamma-1}} \left[1 - \left(\frac{p_e}{p_c} \right)^{\frac{\gamma-1}{\gamma}} \right]} + \frac{c^* \varepsilon}{g_0 p_c} \left(p_e - p_a \right) \right\} \tag{2}$$

$$c^* = \frac{\eta_{c^*}\sqrt{\gamma R T_c}}{\gamma\left(\frac{2}{\gamma+1}\right)^{\frac{\gamma+1}{2\gamma-2}}} \tag{3}$$

$$\frac{p_e}{p_c} = \left[1+\frac{\gamma-1}{2}M_e^2\right]^{\frac{\gamma}{1-\gamma}} \tag{4}$$

$$\varepsilon = \frac{1}{M_e}\left[\left(\frac{2}{\gamma+1}\right)\left(1+\frac{\gamma-1}{2}M_e^2\right)\right]^{\frac{\gamma+1}{2\gamma-2}} \tag{5}$$

The exit Mach number (M_e) may be determined implicitly from the nozzle expansion ratio (set by the nozzle design) via equation (5). With the combustion chamber pressure set, the mass flow required may be determined from the thrust goal, the target I_{sp} and the relation $I_{sp} = F/W$.[7] The pump head required may be determined from the sum of the pressure drops through the cooling system, the injector, and the turbine; the last of these may be found if the turbine pressure ratio is known. Thus equation (1) was solved iteratively for the turbine pressure ratio with the seven following assumptions:

1. Oxygen behaves ideally at all operating conditions experienced by the pump
2. the pump has a total efficiency of 85%
3. the turbine has an efficiency of 90%
4. combustion chamber pressure of 1,740 psi (12 MPa) calculated based on goal I_{sp}
5. total pressure drop of 20% in the cooling jacket and 300 psi (2.07 Mpa) between the turbine exhaust and combustion chamber (includes injector pressure loss)

6. a thrust requirement of 50,000 lb_f (222 kN)

7. target I_{sp} specified in Phase III IHPRPT goals.

Combined with results from NASA's Numerical Propulsion Simulation System (NPSS)[37], this analysis yielded the design point values for pump and turbine characteristics listed in Table 7. The design process is illustrated in Figure 7.

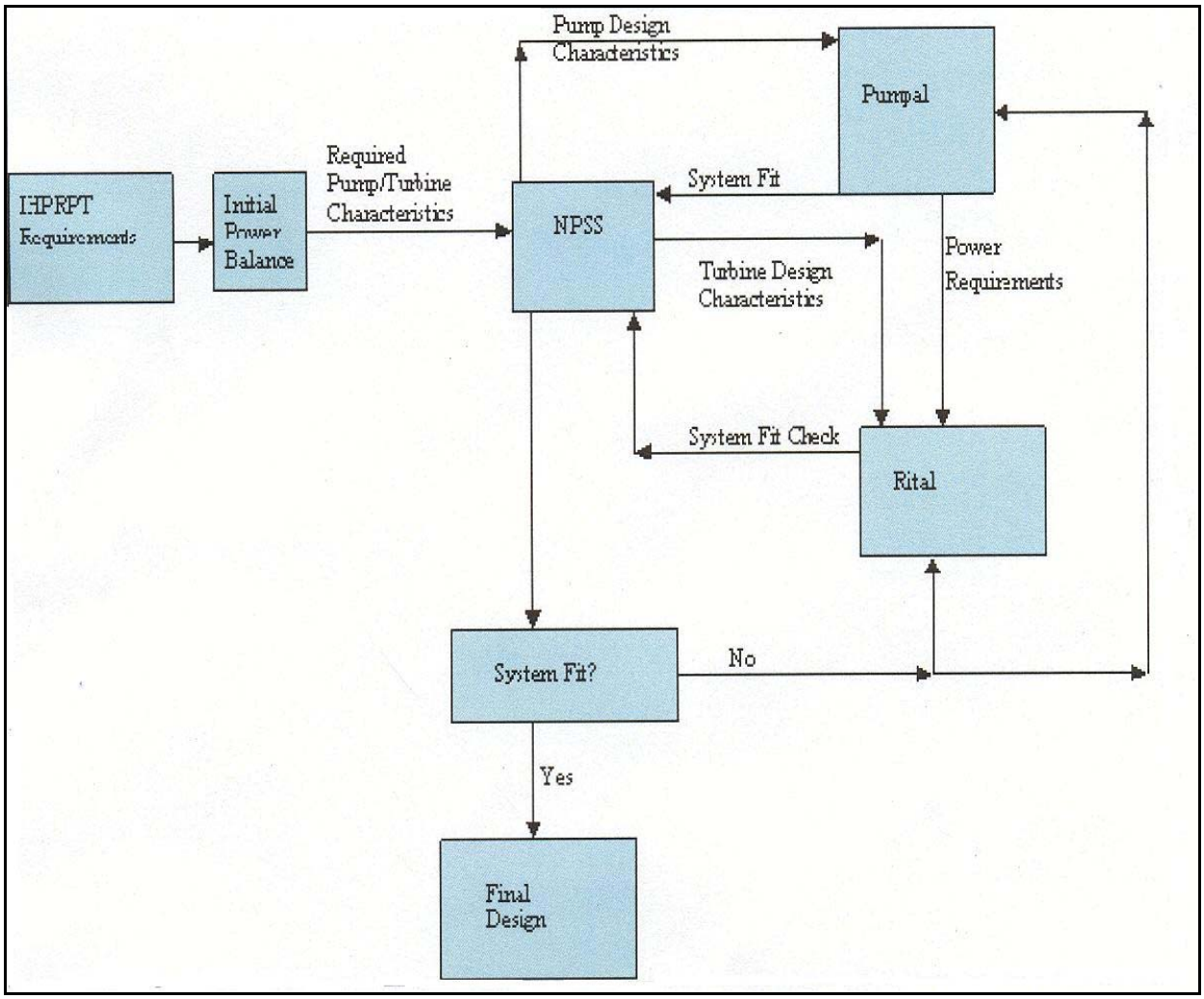

Figure 7: Design process block diagram

Table 7: Turbopump design point

Pump inlet pressure, psi (Mpa)	45 (.31)
Pump output pressure, psi (Mpa)	4500 (31)
Mass flow, lbm/s (kg/s)	106 (48.1)
Turbine inlet total pressure, psi	3663 (25.26)
Turbine total pressure ratio	1.8
Turbine inlet total temperature, R (K)	600 (333)
Shaft speed, rpm	32000

3.2 Pump Design

To aid in the detailed design of the impeller, the Concepts NERC software package Pumpal[38] was used. This package uses a mean line (mass averaged one dimensional analysis along a streamline) code to size and predict the pump performance. This software may be operated in two modes of interest for this work: design (which is used to create impellers and determine performance at the design point) and analysis (which is used to determine off-design characteristics and draw the pump maps shown in chapter 4). Inputs to the program are shown in Table 8 below.

Table 8: Pumpal inputs

Inlet total pressure, psi (MPa)	45 (0.31)
Inlet total temperature, ^{o}R (K)	150 (83.3)
Inlet mass flow, lbm/s (kg/s)	106 (48.08)
Speed, rpm	32000
Total Dynamic Head, psi (MPa)	4500 (31.03)
Impeller inlet incidence angle (hub)	2^{o}
Impeller inlet incidence angle (mean)	2^{o}
Impeller inlet incidence angle (tip)	2^{o}
Impeller inlet blade number	7
Leading edge blade thickness, in (mm)	.0625 (1.588)
Inclination angle at impeller exit	90^{o}
Impeller exit blade number	14

The impeller inlet and exit blade numbers were chosen based on the guidance in Oyama and Liou[32] so as to maximize the total head produced by the pump and minimize power required. The incidence values were chosen to be small in accordance with the guidance in Japikse, Marscher, and Furst[39] to prevent flow separation and stalling at the inlet and to help ensure a wide throttling range.

3.2.1 Impeller Inlet

In order to determine optimum impeller dimensions, Pumpal was run in design mode, which first sets the impeller inlet tip radius (the optimum value of which corresponds to minimum tip relative speed) via the following equation[40]:

$$R_{1t} = \left(\frac{30Q\sqrt{2}}{\pi^2 N(1-(R_{1h}/R_{1t})^2)} \right)^{1/2} \tag{6}$$

where N is the pump's rotational speed, Q is the volumetric flow rate, R_{1h} is the inlet hub radius, and R_{1t} is the inlet tip radius. This equation assumes no inlet swirl, and the inlet hub-to-tip ratio is fixed. In order to determine this, the impeller eye is sized to obtain the minimum Net Positive Suction Head Required (NPSH):

$$NPSH = \frac{1}{2}\rho C_{1t}^2(1+\sigma_b) + \frac{1}{2}\sigma_b U_{1t}^2 \tag{7}$$

Where ρ is the inlet density, C_{1t} is the absolute flow velocity at the tip inlet, U_{1t} is the blade tip speed at the inlet, and σ_b is the slip factor, which is assumed constant. By minimizing the NPSH requirement, the designer allows himself a greater range of cavitation-free flow and thus a larger potential operating range for the pump.

Minimum NPSH then occurs when:

$$R_{1t}^2 = R_{1h}^2 + \left[\left(\frac{30}{\pi N} \right)^2 \frac{2Q^2}{\pi^2} \frac{1+\sigma_b}{\sigma_b} \right]^{\frac{1}{3}} \quad (8)$$

The blade angle is then set by:

$$\beta_{1tb} = \beta_{1t} + I_{1t\_opt} \quad (9)$$

$$\beta_{1mb} = \beta_{1m} + I_{1m\_opt} \quad (10)$$

$$\beta_{1hb} = \beta_{1h} + I_{1h\_opt} \quad (11)$$

The subscripts t, m, and h correspond to the tip, mean, and hub respectively, β_b is the blade angle, β is the flow angle, and I is the incidence specified in Table 8.

3.2.2 Impeller Outlet

The impeller outlet calculation scheme selected optimizes the impeller outlet radius and impeller exit width. The outlet radius is adjusted to match the desired head rise, while the exit width is based on the value of the exit swirl parameter (defined as the ratio of the tangential to meridional velocities).

3.2.3 Volute

To begin the volute calculation scheme, a loss coefficient (LC57) is determined, where LC57 is the sum of a meridional (LC_m) and tangential loss coefficient (LC_t), total loss of the meridional component of the entering kinetic energy is assumed, and:

$$LC_m = \frac{1}{1+\lambda^2} \quad (12)$$

$$LC_t = \left(\frac{r_5}{r_6} \right)^2 \frac{\left(\lambda - 1/AR\right)^2}{1+\lambda^2} \quad (13)$$

Here λ, the inlet swirl parameter, is defined as the ratio of the tangential and meridional velocities at the volute inlet (station 5), AR is the ratio of the volute throat area to the volute inlet area, and LC_t is the average of the inlet and throat radii; if the core flow accelerates ($C_{t5} < C_7$) as happens in the design case, there is no loss in the tangential velocity component and so LC_t becomes zero. After LC57 is determined, other properties at the volute throat (station 7) may be determined as follows:

$$P_{07} = P_{05} - LC57 * (P_{05} - P5) \tag{14}$$

$$T_{07} = f(P_{07}, H_{05}) \tag{15}$$

$$s = f(P_{07}, T_{07}) \tag{16}$$

Static properties at the volute throat (station 7) are then calculated in an iteration loop using equations (17)-(21):

$$C_t = \frac{M}{A_7 * \rho_7} \tag{17}$$

$$H_7 = H_{05} - \frac{C_t^2}{2} \tag{18}$$

$$P_7 = f(H_7, s) \tag{19}$$

$$T_7 = f(H_7, P_7) \tag{20}$$

$$\rho_7 = f(T_7, P_7) \tag{21}$$

The pressure recovery coefficient at the volute exit (station 8) is determined by a blockage correlation model, illustrated in Figure 8, which assumes a blockage of 12% at the volute throat. Once this coefficient (CP78) is determined, other properties may be determined in an iterative process as done for station 7:

$$P_8 = P_7 + CP78 * (P_{07} - P_7) \tag{22}$$

$$H_{08} = H_{07} \tag{23}$$

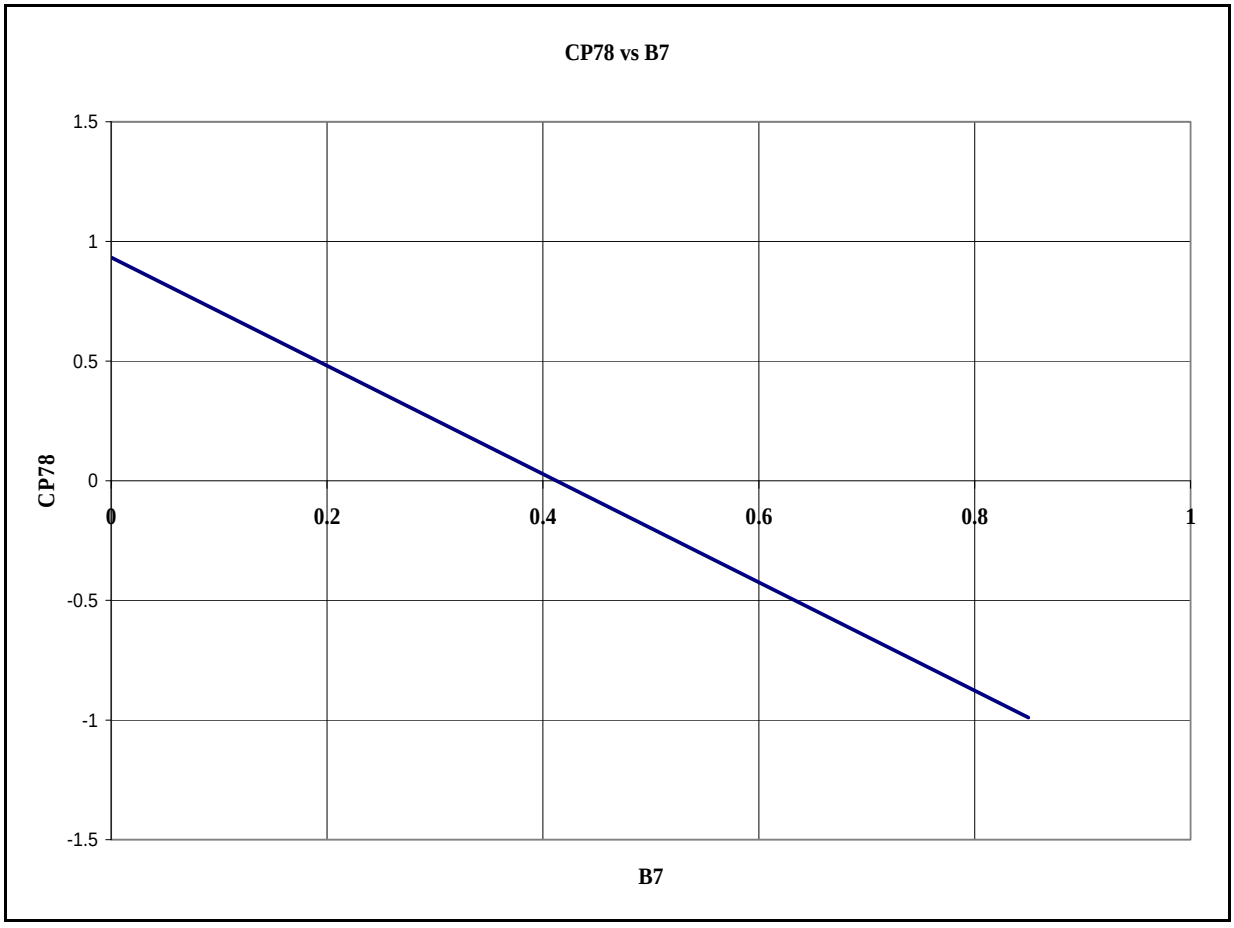

Figure 8: Blockage correction for Station 8 pressure recovery[40]

3.2.4 Analysis Mode

In order to determine off-design performance and draw the pump maps presented in Chapter 4, Pumpal must be run in analysis mode. In this mode, the total pressure and temperature at the impeller inlet are fixed from the upstream conditions and the velocity triangles and static conditions are solved via an iterative process using equations (24) to (29):

$$P_{01} = \left(P_{\infty} + LC1 * P_1\right)/(1 + LC1) \tag{24}$$

$$h_{01} = h\left(T_{\infty}, P_{\infty}\right) \tag{25}$$

$$s_1 = s\left(h_{01}, P_{01}\right) \tag{26}$$

$$C_{m1} = \frac{\dot{m}}{\rho_1 A_1 \left(1 - B1\right)} \tag{27}$$

$$C_1 = C_{m1} / \cos\left(\alpha_1\right) \tag{28}$$

$$h_1 = h_{01} - \frac{1}{2} C_1^2 \tag{29}$$

$$\rho_1 = \rho\left(h_1, s_1\right) \tag{30}$$

LC1 is the upstream loss coefficient, B1 is the upstream blockage, α_1 is the inlet flow angle, A_1 is the impeller inlet area, $\dot{m}$ is the mass flow, C_1 is the impeller inlet absolute velocity, C_{m1} is the impeller inlet meridional velocity (both at the RMS position), and ρ, h, and s symbolize density, enthalpy, and entropy, respectively, which are calculated based on NIST data.

A two-zone model is used to determine the conditions at the impeller exit. This model divides the outlet flow into two zones (primary and secondary), and employs these basic assumptions:

1. The primary zone flow is assumed to be isentropic; all losses inside the impeller passage occur in the secondary zone.
2. At the impeller exit, the primary zone and secondary zone have the same static pressure.

The first step in this process is to calculate the relative velocity in the primary zone:

$$W_{2p} = W_{1t} * DR2 \tag{31}$$

W_{2p} is the primary zone relative velocity at the impeller exit, W_{1t} is the relative inlet velocity at the impeller tip, and DR2 is the diffusion ratio, defined by:

$$DR2 = \frac{W_{1t}}{W_{2p}} \tag{31}$$

The value of DR2 is determined by a specific speed function, illustrated in Figure 9 (with the specific speed given in the figure in English units) which has been derived from past pumps. With W_{2p} known, the assumption of rothalpy conservation[41] is applied, as explained below.

If the flow through a thin annular passage bounded by two stream surfaces is analyzed, the torque (τ) acting on the fluid between two meridional locations is given by the conservation of angular momentum[42]:

$$\tau = \dot{m}\,(r_2 C_{\theta 2} - r_1 C_{\theta 1}) \tag{32A}$$

With r being the radius at each station, and C_θ being the absolute tangential flow velocity. The power imparted to the fluid is then the product of this torque and the angular velocity Ω[41]:

$$\tau\ \Omega = \dot{m}\,(U_2 C_{\theta 2} - U_1 C_{\theta 1}) \tag{32B}$$

The work done on the fluid per unit mass (specific work) is the power divided by the mass flow rate, or $U2C_{\theta 2} - U_1 C_{\theta 1}$.

Since the specific work done on the fluid is equal to the change in total enthalpy for steady, adiabatic, and irreversible flow,

$$h_{02} - h_{01} = U_2 C_{\theta 2} - U_1 C_{\theta 1} \tag{32C}$$

With total enthalpy defined as $h_0 = h + 0.5C_1^2$ equation (32C) may be rearranged to give[41]:

$$h_1 + 0.5C_1^2 - U_1 C_{\theta 1} = h_2 + 0.5C_2^2 - U_2 C_{\theta 2} = I$$

Where I is defined as the rothalpy (rotational stagnation enthalpy), a quantity that is unchanged between impeller entrance and exit.

Applied here, the assumption of constant rothalpy gives:

$$h_{2p} + \frac{W_{2p}^2}{2} - \frac{U_2^2}{2} = h_1 + \frac{W_1^2}{2} - \frac{U_1^2}{2} \tag{33}$$

This may be rearranged to find the static enthalpy:

$$h_{2p} = \left(h_1 + \frac{W_1^2}{2} - \frac{U_1^2}{2} \right) - \frac{W_{2p}^2}{2} + \frac{U_2^2}{2} \tag{34}$$

Since the flow in the primary zone is assumed to be isentropic,

$$s_{2p} = s_1 \tag{35}$$

With s_{2p} and h_{2p} known, other thermodynamic properties such as P_{2p}, T_{2p}, and ρ_{2p} may be determined. The primary flow angle (β_{2p}) may then be found from the impeller exit blade angle (β_{2b}) and the deviation angle (δ_{2s}) from equation (36):

$$\beta_{2p} = \beta_{2b} + \delta_{2s} \tag{36}$$

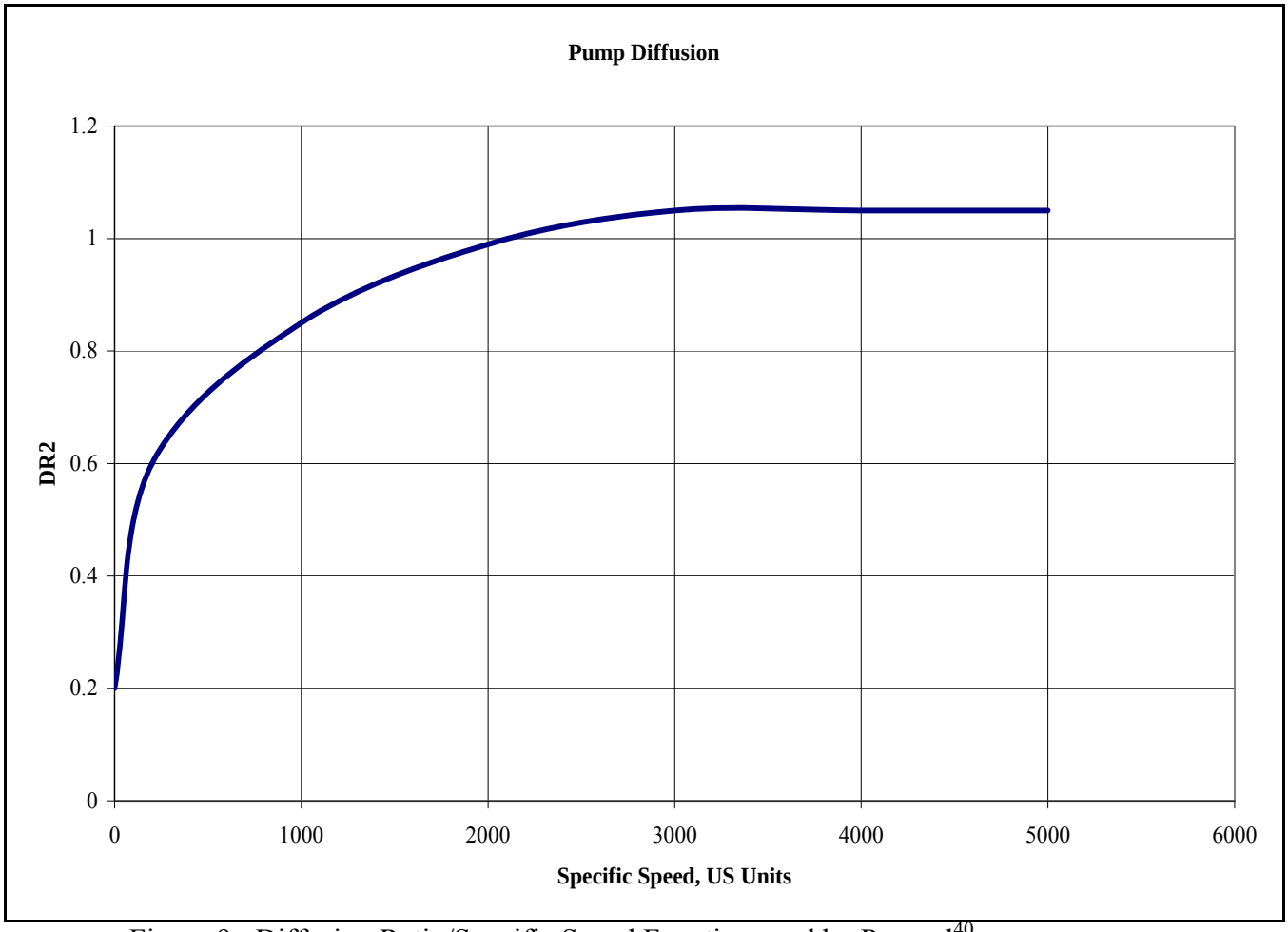

Figure 9: Diffusion Ratio/Specific Speed Function used by Pumpal[40]

The velocity triangle is completely defined with β_{2p} and W_{2p}. After the primary zone has been completely defined, the mass fraction in the primary zone may be calculated:

$$1-\chi = \frac{\rho_{2p}(1-\varepsilon)A_2 W_{2p}\cos(\beta_{2p})}{\dot{m}} \tag{37}$$

where the secondary flow mass fraction (χ, which is determined by the program as a function of specific speed) is defined as:

$$\chi = \frac{\dot{m}_s}{\dot{m}_{tot}} \tag{38}$$

where the subscripts s and tot refer to the secondary and total flows, respectively, and the secondary area fraction (ε) is defined as:

$$\varepsilon = \frac{A_{2s}}{A_2} \tag{39}$$

The secondary area fraction may be found from:

$$\varepsilon = 1 - \frac{(1-\chi)\dot{m}}{\rho_{2p}A_2 W_{2p}\cos(\beta_{2p})} \tag{40}$$

Also, since

$$\chi = \frac{\rho_{2s}(\varepsilon A_2)W_{2s}\cos(\beta_{2s})}{\dot{m}} \tag{41}$$

the secondary zone relative velocity (W_{2s}) may be found from:

$$W_{2s} = \frac{\chi \dot{m}}{\varepsilon \rho_{2s} A_2 \cos(\beta_{2s})} \tag{42}$$

With W_{2s} known, conservation of rothalpy[41] may be applied in a similar fashion to the primary zone in order to determine the static enthalpy of the secondary zone:

$$h_{2s} = (h_2 + \frac{W_1^2}{2} - \frac{U_1^2}{2}) - \frac{W_{2s}^2}{2} + \frac{U_2^2}{2} \tag{43}$$

With the secondary zone static pressure known from assumption 2 above (equal static pressures in both zones), all the thermodynamic properties may be determined.

The secondary flow angle may then be determined from the impeller exit blade angle and the secondary deviation angle (δ_{2s}):

$$\beta_{2s} = \beta_{2b} + \delta_{2s} \tag{44}$$

With W_{2s} and β_{2s} known, the velocity triangle for the secondary zone is fully defined. The primary and secondary zones are assumed to mix instantly and uniformly at the impeller exit. The mass and momentum conservation equations that apply to this situation are as follows:

$$\rho_{2m} C_{M2m} A = \rho_{2p} C_{M2p} (1-\varepsilon) A + \rho_{2s} C_{M2s} \varepsilon A \tag{45}$$

$$(P_{2p} - P_{2m}) A = \rho_{2m} C_{M2m}^2 A - \{\rho_{2p} C_{M2p}^2 (1-\varepsilon) A + \rho_{2s} C_{2s}^2 \varepsilon A\} \tag{46}$$

$$C_{t2m} = \chi C_{t2s} + (1-\chi) C_{t2p} \tag{47}$$

The subscript m signifies mixed out conditions. The specific total enthalpy after mixing, h_{02m} , after accounting for power losses from front and rear leakage (P_{fleak} and P_{rleak} , respectively) disk friction (P_{df}), and recirculation(P_{recirc}) is :

$$h_{02m} = h_{02a} + \frac{P_{fleak} + P_{rleak} + P_{df} + P_{recirc}}{\dot{m}} \tag{48}$$

With the fluid's equation of state fixed (this case uses NIST[43] data for Oxygen), equations (45) through (48) may be solved iteratively to determine the conditions after mixing.

3.3 Turbine Design

The Concepts NERC software Rital[44] was used to design the turbine. This software uses a meanline code to predict turbine performance. Initial inputs to the program are shown below:

Table 9: Initial turbine design inputs

Inlet total pressure, psi (MPa)	3663 (25.26)
Outlet total pressure, psi (MPa)	2035 (14.03)
Inlet total temperature, R (K)	520 (288.9)
Shaft speed, rpm	32000
Mass flow, lbm/s (kg/s)	95 (43.09)
Optimum incidence, degrees	-35
Power required, hp (kW)	2215 (1651.7)

The optimum incidence angle was chosen based on the range suggested by Moustapha, et al.[45] and the guidance given by Rohlik[35] based on the need to prevent flow separation in the blade passage and past design experience and experimental results. Other inputs were derived from the power balance and Pumpal design.

3.3.1 Preliminary Sizing

In order to determine initial parameters for the turbine, Rital was run in preliminary design mode, which requires the user to specify three of the following conditions: inlet total pressure, exit static pressure, mass flow rate, and power. Since the

power requirement, inlet total pressure, and mass flow were determined in the power balance and fluid-end design, these properties were chosen.

The preliminary sizing algorithm[46] uses a specified optimum flow coefficient (ϕ, defined in equation (49) below) and loading coefficient (ψ, defined in equation (50) below):

$$\phi = \frac{C_{M6}}{U_4} \tag{49}$$

$$\psi = \frac{\Delta h_0}{U_4^2} \tag{50}$$

where C_{M6} is the rotor exit meridional velocity, U_4 is the rotor tip speed, and Δh_0 is the actual specific enthalpy change. The value of ϕ was chosen to be 0.25 for maximum efficiency as suggested by the program and echoed by Mathis[47] based on past design experience. The loading coefficient was chosen to be 0.9, as suggested by the program based on past results[46]. After the rotor inlet radius is found, RITAL proceeds to calculate the rest of the nozzle and rotor geometry as follows.

The velocity triangle at the rotor outlet is found by assuming a rotor meridional velocity ratio, ξ, of unity and zero exit swirl; along with a specified incidence, this sets the rotor inlet angle. Continuity considerations then determine the blade inlet width.

The selected ϕ may be used along with the assumption of zero exit swirl to determine the rotor exit area and thus the exit tip radius; the ratio of rotor exit hub radius to rotor inlet radius is set to 0.3. The exit blade angle is calculated with an assumed deviation angle, δ_6, of 5 degrees. The axial length (AxLen) is found from the relations below:

$$\frac{\text{AxLen}}{\text{R}_4} = 0.6 \text{ , for } \frac{R_{6s}}{\text{R}_4} > 0.7 \tag{51}$$

$$\frac{\text{AxLen}}{\text{R}_4} = 0.4 \text{ , for } \frac{R_{6s}}{\text{R}_4} < 0.4 \tag{52}$$

Intermediate values are found by linear interpolation. The blade thickness is set as two percent of the tip radius, while inlet and outlet clearances are set at one percent of the inlet blade height.

The nozzle exit to rotor inlet radius is fixed at 1.05; the velocity triangle is determined from conservation of mass and angular momentum from rotor inlet. The blade angle is then found assuming a two degree deviation angle. The nozzle inlet ratio is then set as 1.25 times the nozzle exit ratio. The nozzle exit blade angle is either set to zero or calculated assuming a straight blade, depending on the deviation model selected; in this case a straight blade was assumed. Results of this step are listed in Table 11 in Chapter 4.

3.3.2 Final Design

After completion of preliminary sizing, RITAL was run in a design mode that required the user to input the exit total pressure (known in this case from the initial power balance) and returned the nozzle exit blade angle. This mode was used to create the final design and to set such parameters as the number of nozzle and rotor blades, axial and radial clearances, and rotor exit hub-to-tip ratio.

The number of nozzle blades selected was based on a relation given by Mathis[47]:

$$Z = \frac{(b/s)2\pi r_m}{t_{te}/\cos(\alpha_{te})}\delta_6 \tag{53}$$

where (b/s) is the blockage ratio, r_m is the mean radius, t_{te} is the trailing edge thickness, and α_{te} is the flow angle.

To determine the number of rotor blades, a relation presented by Rohlik[35] to determine the minimum number of blades necessary to prevent flow separation was used:

$$n = 0.03(\alpha_1 - 57)^2 + 12 \tag{54}$$

Where n is the minimum number of rotor blades and α_1 is the nozzle exit flow angle in degrees as determined in the previous step.

The axial clearance was chosen to be one percent of the inlet blade height (due to manufacturability concerns) and the radial clearance was chosen to be one half of one percent of the exit blade height to maximize total efficiency in light of the results presented by Futral and Holeski[48] who found that the deleterious effect of increasing radial clearance on total efficiency was ten times greater than an equal percentage increase in axial clearance. In accordance with the guidance in Mathis[47] the rotor exit hub-to-tip ratio was chosen to be about 0.33 to enable the use of a smaller and less expensive rotor.

Nozzle losses were modeled by a user-specified loss coefficient that is used to calculate the difference between actual and ideal static enthalpy at the trailing edge of the nozzle. Based on guidance presented in the program and by Dixon[41] for well designed nozzle rows in normal operation, this was chosen as 0.04.

The deviation in the nozzle, δ, was modeled using a modification to the Howell correlation proposed by Jansen[49]:

$$\delta = \alpha_3 - \alpha_{b3} = a_3(\alpha_{b3} - \alpha_{b1})\frac{\pi(r_1 + r_3)}{Z_N * C} \tag{55}$$

where a_3 is a constant, chosen as 0.13, α_3 is the nozzle exit flow angle, α_{b3} is the nozzle exit blade angle, α_{b1} is the nozzle inlet blade angle, r_1 and r_3 are the nozzle inlet and outlet radii, respectively, Z_N is the number of nozzle blades, and C is the blade cord.

There are four types of rotor losses modeled by the program: clearance, incidence, trailing edge, and passage losses. These are detailed below.

Passage losses in the rotor are modeled using a NASA loss model that calculates the passage loss as a fraction of the mean passage kinetic energy:

$$L_p = \frac{1}{2}K_p(W_4^2 \cos^2 i + W_5^2) \tag{56}$$

where i is the angle between the incoming flow and that at the best efficiency point, L_p is the passage loss, W_4 is the relative velocity at the rotor entrance, W_5 is the relative velocity at the rotor exit and K_p is an empirical coefficient whose value is set at 0.3.

Incidence losses (L_i) are modeled as the loss of tangential kinetic energy as the flow turns from the inlet flow angle to the angle at the best efficiency point:

$$L_i = \frac{1}{2}W_4^2 \sin^2 i \tag{57}$$

Clearance losses (L_c) are assumed to be a function of the clearance/ blade height ratio:

$$L_c = K_c\left(\frac{\varepsilon_r}{b_5}\right) \tag{58}$$

Here ε_r is the exit clearance and b_5 is the outlet blade height.

4 Results

This chapter presents and discusses the results of the DEAN Oxygen pump design study. Concepts NERC's Pumpal[38] and Rital[44] programs were used to model the pump and turbine, respectively. This pump was designed to enable the DEAN to achieve IHPRPT Phase III performance and logistics goals and was required to deliver 106 lb/s (48.08 kg/s) LOX at a pressure of 4,500 psi (31.03 MPa) based on the power balence. Inputs to Pumpal and Rital are listed in Appendix A.

4.1 Pump Results

The final pump design and performance parameters are listed in Table 10; angles listed are measured using the meridional convention. This pump will deliver 106 lbm/s (48.08 kg/s) LOX at a total pressure of slightly over 4600 psi (31.7 MPa) while demanding a power input of 2215 hp (1651 kW). Figure 10 is an illustration of the final impeller.

Table 10: Pump design and performance parameters

Total Inlet Pressure, psi (MPa)	45 (.31)
Total Inlet Temperature, R (K)	150 (83.3)
Mass Flow, lbm/s (kg/s)	106 (48.08)
Volumetric Flow rate, ft^3/s (m^3/s)	1.45 (0.041)
Rotational Speed, RPM	32000
Inlet Blade Number	7
Outlet Blade Number	14
Inlet Blade Angle, mean, degrees	-74.376
Outlet Blade Angle, degrees	-59.98
Total Exit pressure, psi (MPa)	4635 (31.96)
Total Head Rise, ft (m)	9013 (2747)
η_{t-t}, %	77.3
Net Positive Suction Head, ft (m)	67 (20.4)
Non-dimensional Specific Speed	0.322

Figure 10: Final impeller

The final design speed was chosen as a compromise between the desire to have a smaller pump (which would argue for a faster rotational speed) and the necessity to avoid excessive friction heating in the pump or turbine that could lead to catastrophic pump failure (which would dictate a lower speed). As pointed out by Campbell and Farquhar[19] other limits on shaft speed which should be considered include allowable stresses, gear and seal velocities, and optimum specific speed. The speed chosen (32,000 rpm) is in the range of current state of the art LOX pumps and should be attainable.[6,13,15]

Figure 11 is the pump head/flow curve. Based on the guidance in NASA SP-8107[11] that a pump-engine system becomes unstable when the slope of the head/flow lines are positive, this pump will be capable of throttling down 32 per cent from its maximum flow at design speed. Its total throttling range (down to half the design speed)

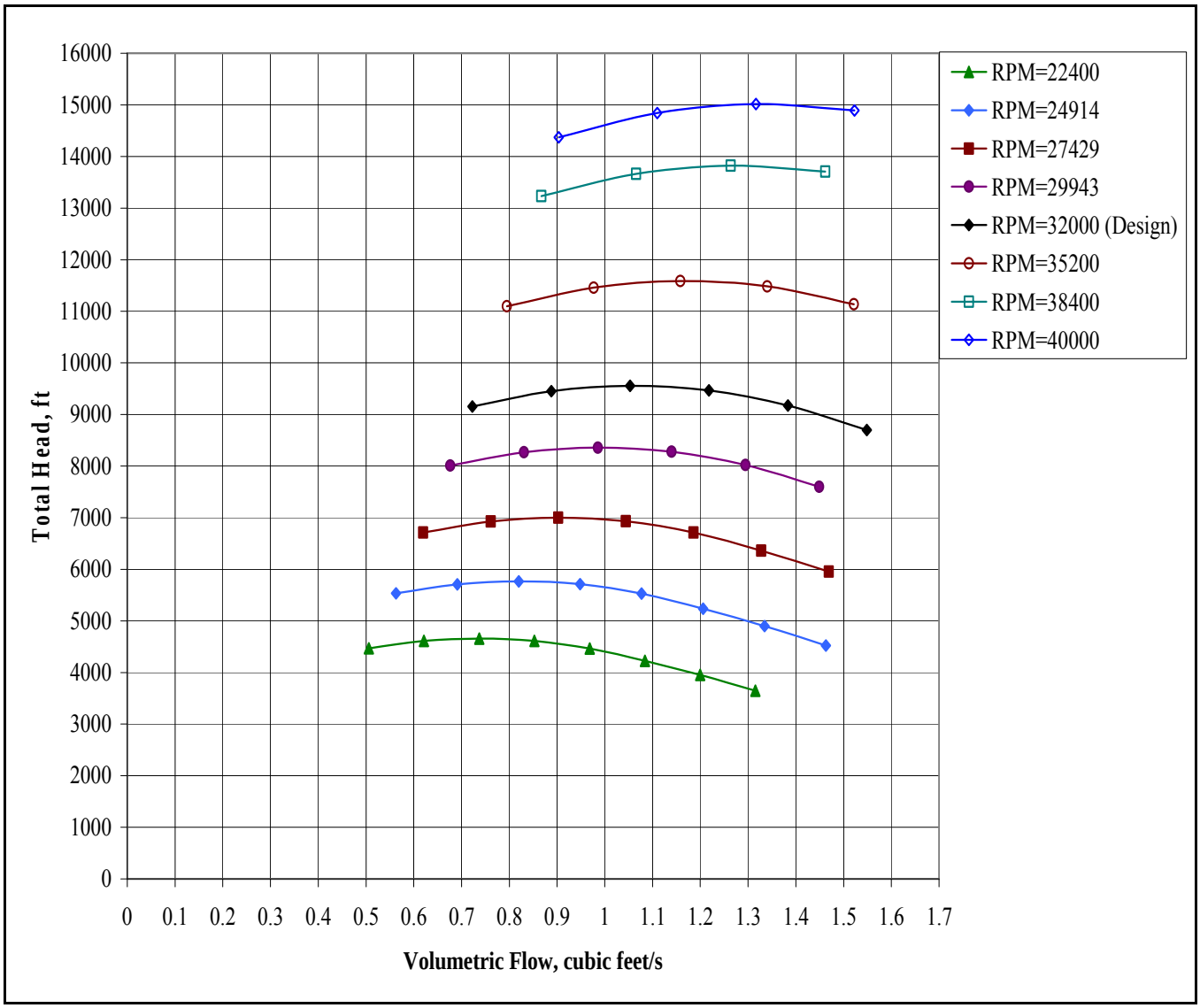

Figure 11: Pump overall performance map

will be 66%. The true lower boundary will depend on pressure losses in the cooling jacket which will decrease as the volumetric flow and thus flow velocity decrease. Figure 13 shows the pump's head/flow behavior and the surge line, which is found by connecting points of zero slope on each of the constant speed lines. The stable operating range is to the right of this line. Given that the pump exit total pressure must be greater than 2,600 psi (17.9 MPa) due to combustion chamber pressure requirements (assuming a

constant pressure loss in the cooling jacket of 20 per cent at all flow conditions), the lowest speed line in Figure 13 likely represents a pressure rise that is of no use to the engine. The lowest useful flow likely obtainable is then 59 lbm/s (26.8kg/s), or 52% of the maximum flow at design speed.

Figure 14 shows the pump's Net Positive Suction Head (NPSH) requirements as a function of flow rate. As expected, these requirements increase as the flow increases. The NPSH available may be calculated by the relation:

$$NPSH = H_{static} + \frac{C_m^2}{2g} - H_{vap} \tag{59}$$

where H_{static} is the static head, C_m is the impeller inlet absolute velocity, and H_{vap} is the head due to vapor pressure. Calculating this quantity using the method suggested by Perry, Green, and Maloney[50] gives an available NPSH of 134 ft (40.8 m) at the design point, against a requirement of 67 ft (20.4 m) as shown by the circled point in Figure 13.

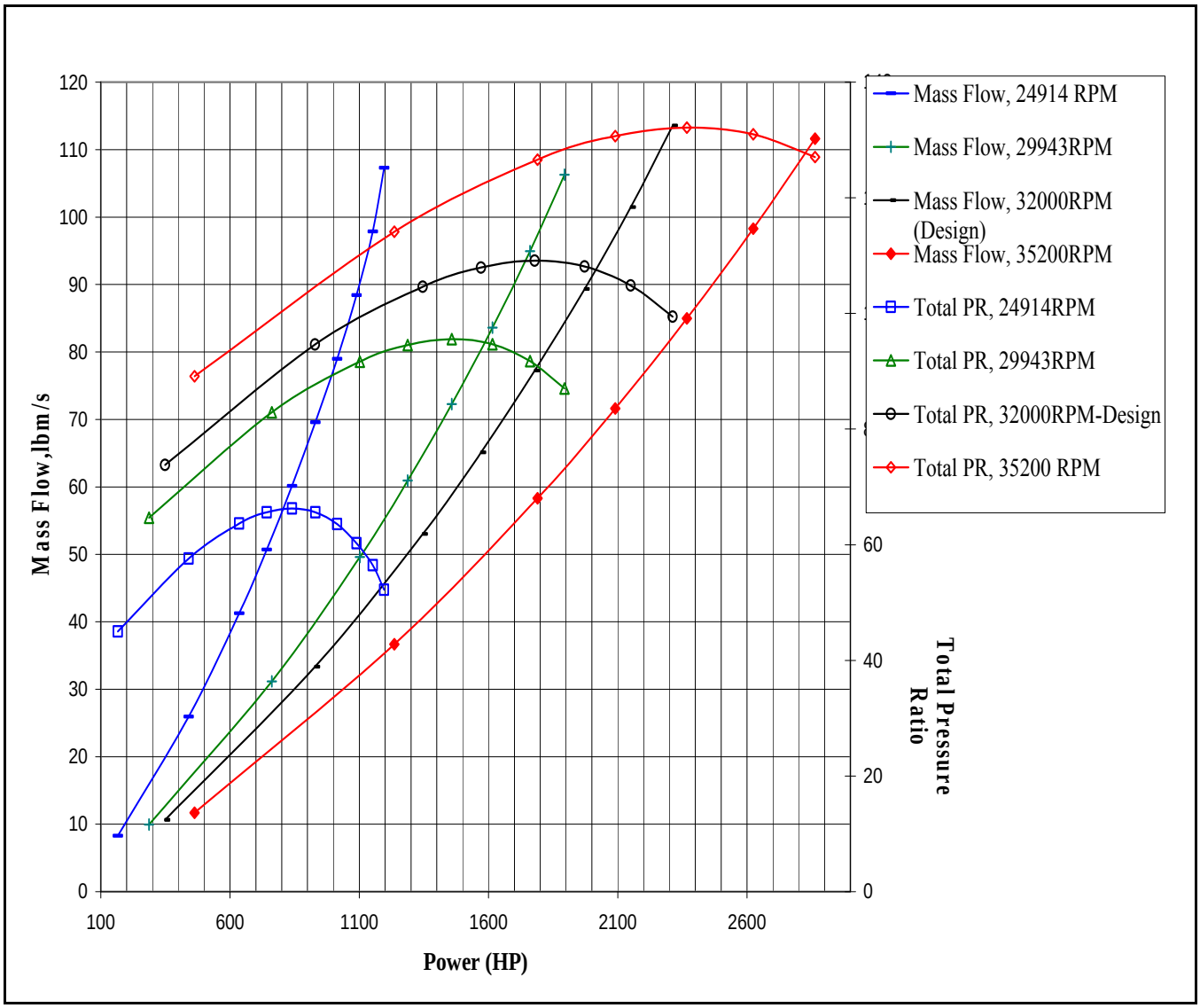

Figure 12: Pump power curve

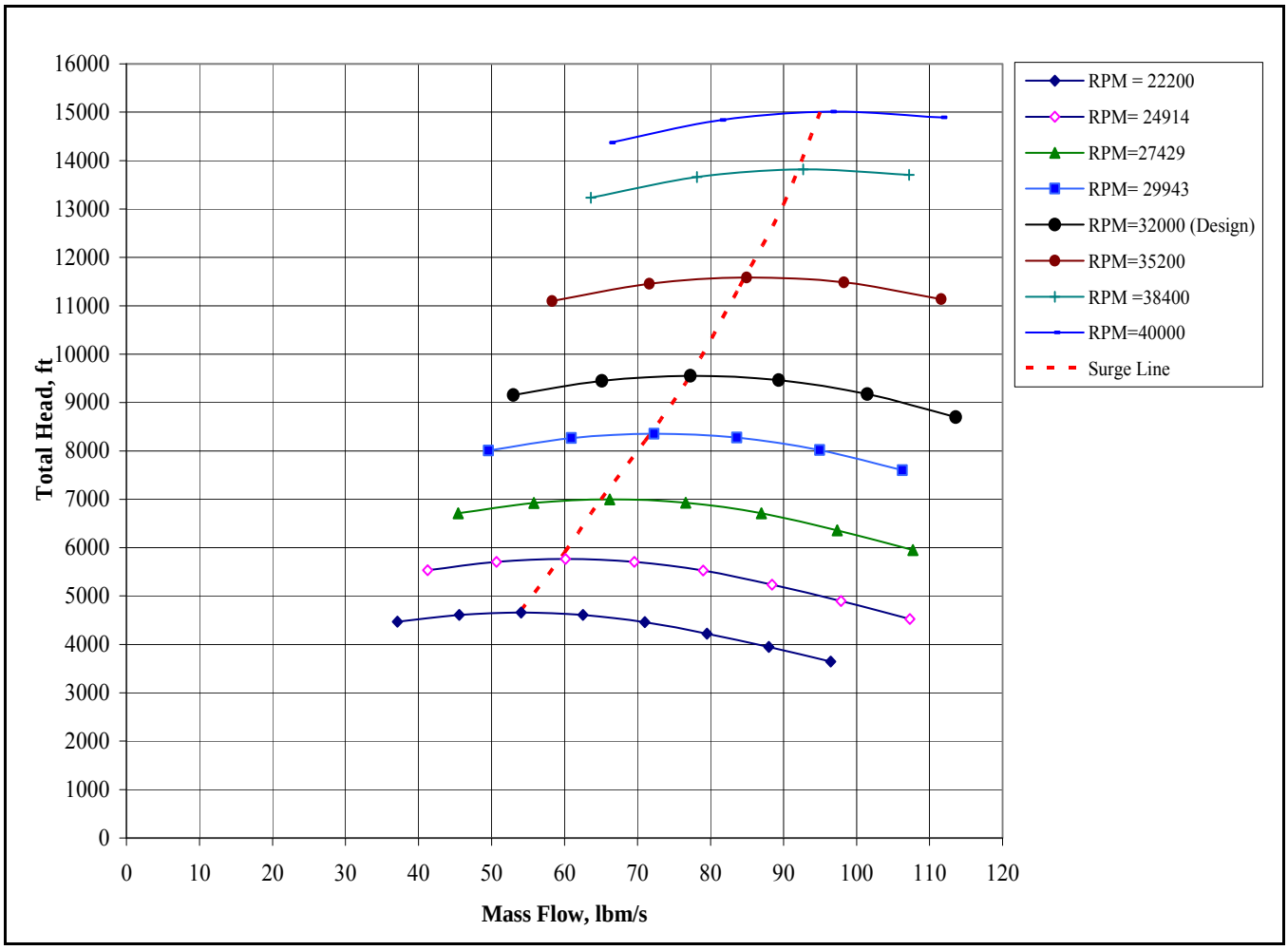

Figure 13: Pump map with surge line

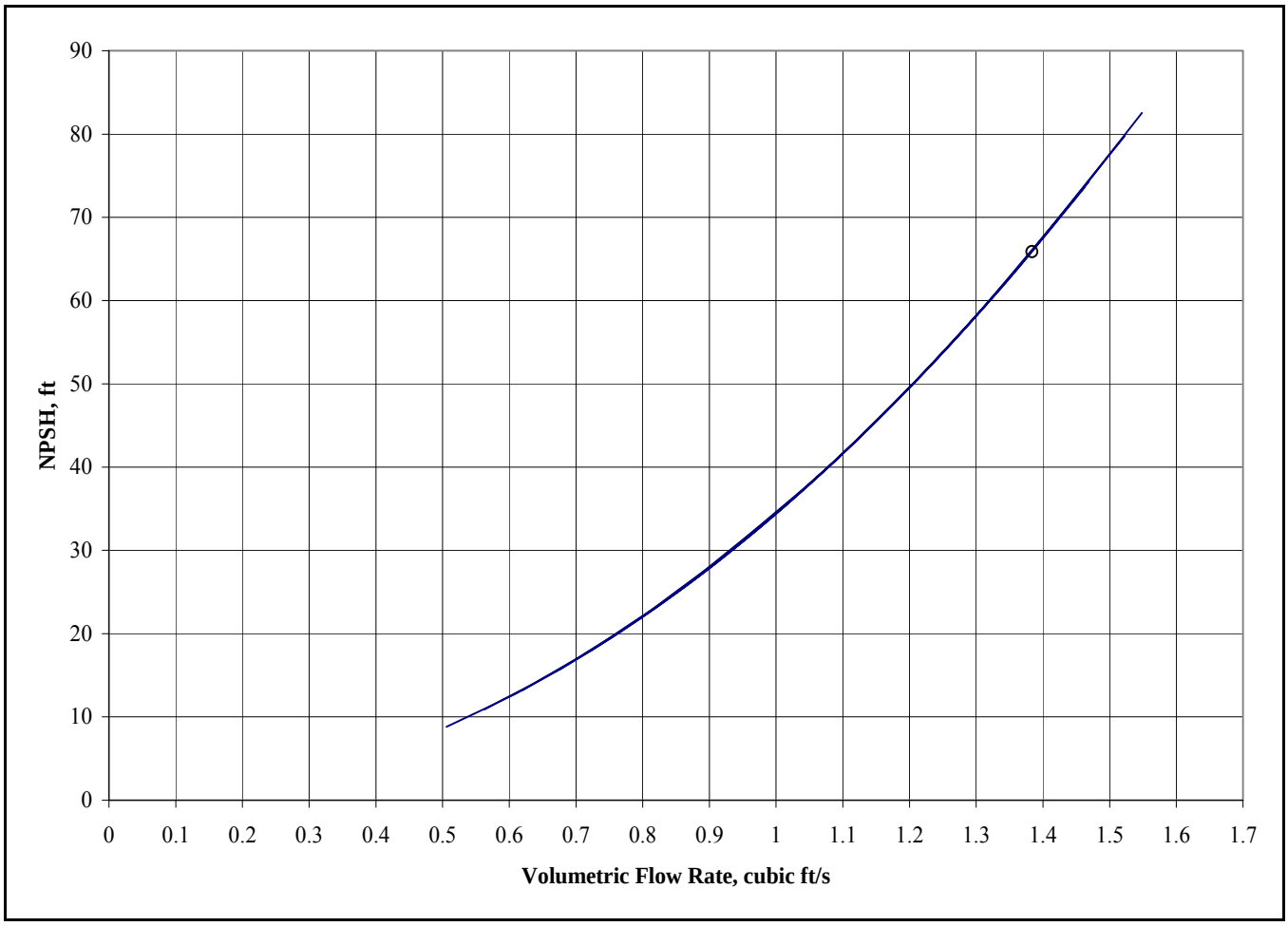

Figure 14: NPSH curve

4.2 Turbine Results

The final turbine design and performance parameters are listed in Table 11. This turbine will supply approximately 10 per cent more power than the pump currently requires; the rotor is illustrated in Figure 15. The specific speed at the design point is very close to the 0.43 suggested by Kofskey and Nusbaum[51] for optimum static efficiency and within the range suggested by them for maximum total efficiency.

Table 11: Turbine design and performance parameters

Total-to-total Pressure ratio	1.80
Total-to-static Pressure ratio	1.98
Inlet Total Temperature, R (K)	600 (333)
Inlet Total Pressure, psi (MPa)	3663 (25.26)
Mass Flow rate, lbm/s (Kg/s)	95 (43.1)
Rotational Speed, RPM	32000
Nozzle Blades	15
Rotor Blades	22
Rotor Hub-to-tip Ratio	0.326
Rotor Exit Blade Angle, degrees	-60
Velocity Ratio, U/C0	0.796
η_{t-t}, %	94.1
η_{t-s}, %	82.6
Non-dimensional Specific Speed	0.438
Power, hp (kW)	2441 (1820)

The turbine's efficiency/velocity ratio curve is shown in Figure 16. The overall trend mirrors that presented by Kofskey and Holeski[52] for a slightly (~7%) larger turbine and is similar to that seen by Kofskey and Wasserbauer[53] for a turbine approximately half as large. The peak total efficiency occurs at a slightly higher value of velocity ratio than that corresponding to the design point, although the difference is slight (roughly one-half of one percent).

Figure 17 shows the corrected mass flow (defined as $\frac{\dot{m}\sqrt{T_0}}{P_0}$) as a function of expansion ratio. The curves seen are typical of subsonic turbines, with mass flow increasing as pressure ratio increases for all speeds; the turbine does not experience choked flow. This indicates that the turbine is not a limiting factor for throttleability.

Figure 18 shows the variation of total efficiency with specific speed; the optimum specific speed for this turbine is 0.465, near that of Kofskey and Nusbaum.[51]

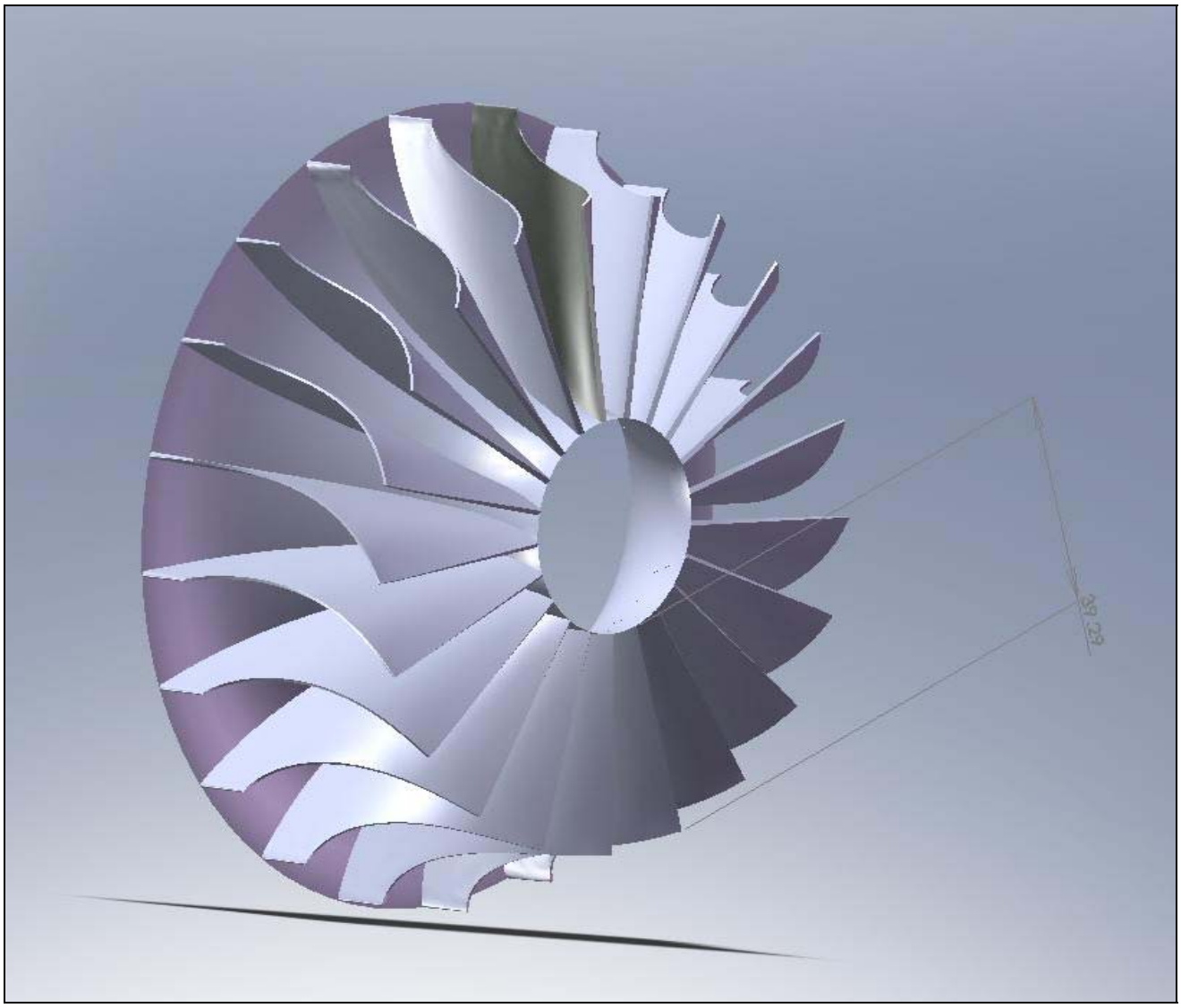

Figure 15: Turbine rotor

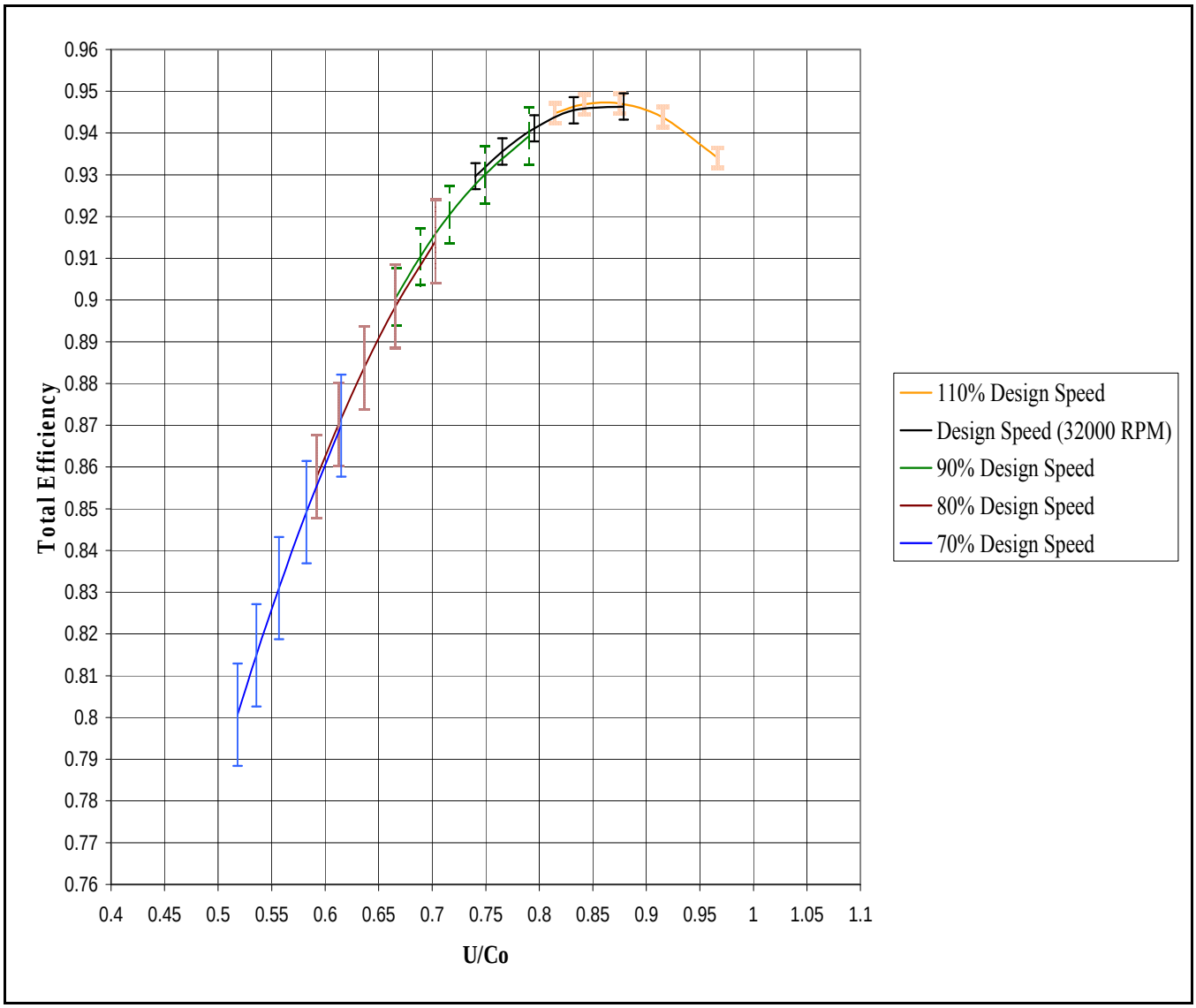

Figure 16: Variation of total efficiency with velocity ratio

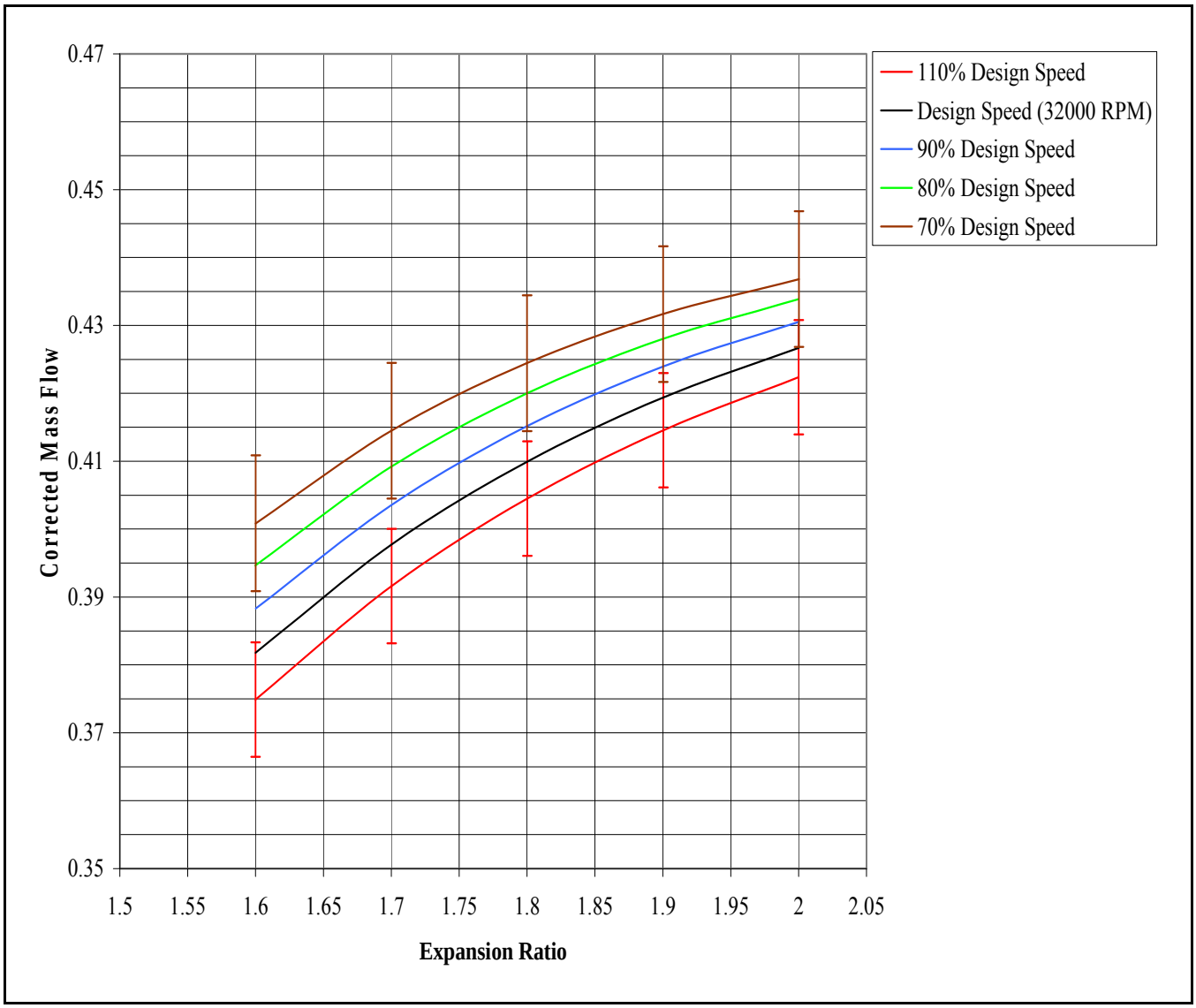

Figure 17: Variation of corrected mass flow with expansion ratio

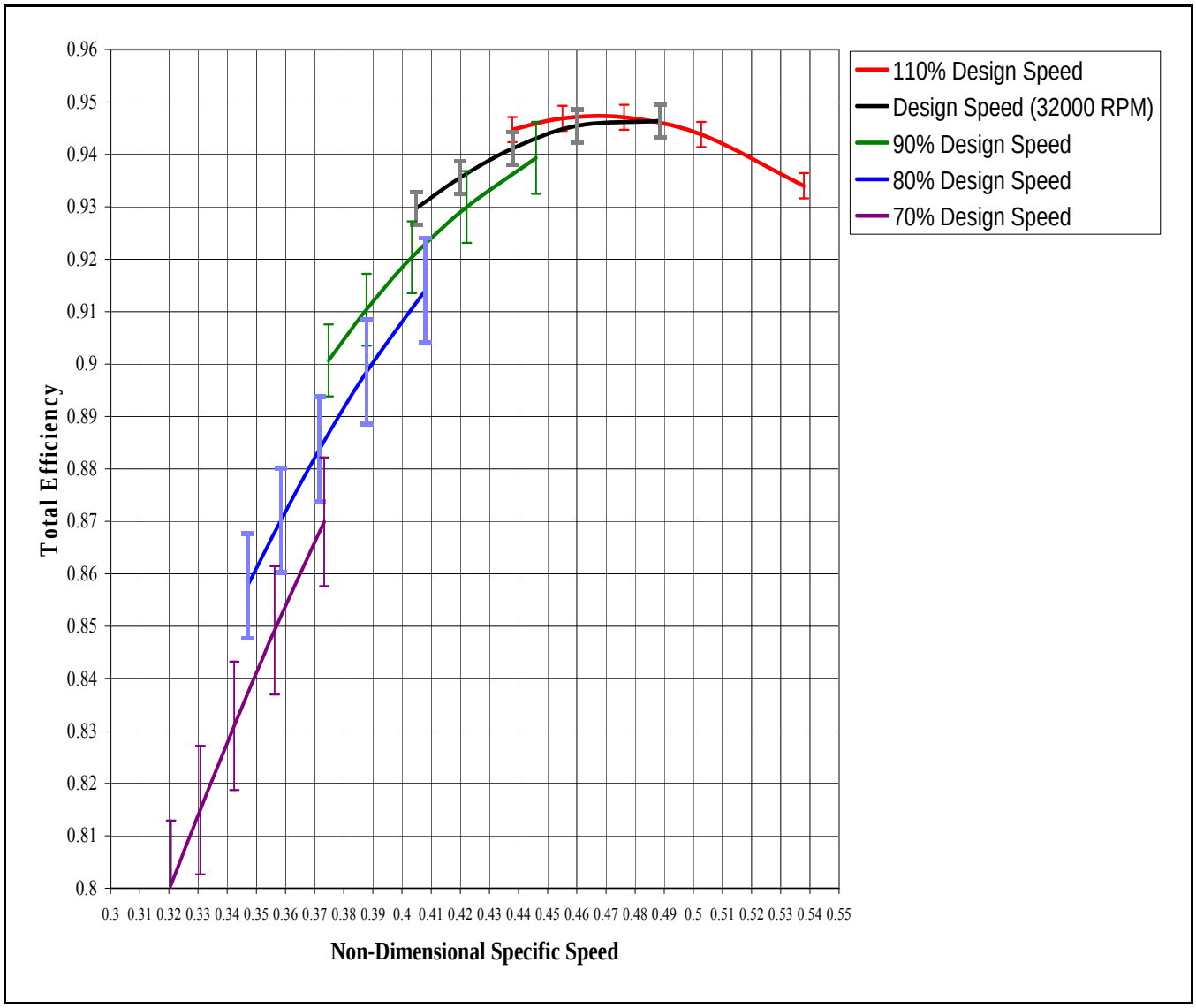

Figure 18: Total efficiency variation with specific speed

4.3 Sensitivity Analysis

In order to determine the most promising areas for future improvement, a sensitivity analysis was done for both the pump and turbine using power as the quantity to be optimized (minimum power requirement for the pump and maximum power output for the turbine); the results of this process are shown in Table 12.

Table 12: Sensitivity Analysis

TURBINE							
Mass flow,lbm/s (Kg/s)	Inlet Tempeature, R (K)	Inlet Pressure, psi (Mpa)	Nozzle blade #	Rotor Blade #	Rotor blade angle,Degrees	Power, HP (kW)	(deltaHP)/ (deltaQ/Q)
95 (43.1)	600 (333)	3663 (25.26)	15	22	-60	2441 (1820)	NA
90 (40.8)	600 (333)	3664 (25.26)	15	22	-60	2313 (1725)	-2432.0
95 (43.1)	568 (315.6)	3665 (25.26)	15	22	-60	2268 (1691)	-3287.0
95 (43.1)	600 (333)	3470 (23.92)	15	22	-60	2246 (1675)	-3705.0
95 (43.1)	600 (333)	3663 (25.26)	14	22	-60	2437 (1817)	-60.0
95 (43.1)	600 (333)	3663 (25.26)	15	23	-60	2434 (1815)	-154.0
95 (43.1)	600 (333)	3663 (25.26)	15	22	-56.84	2431 (1813)	-190.0
PUMP							
Main Blades	Total Blades	Blade Angle	Blade Thickness	RPM	Volute exit diameter ratio	Power, HP (kW)	(deltaHP)/ (deltaQ/Q)
7	14	-59.98	0.1	32000	2	2215 (1652)	NA
6	12	-59.98	0.1	32000	2	2225.451 (1660)	73.2
7	7	-59.98	0.1	32000	2	2249.402 (1677)	68.8
7	14	-56.82	0.1	32000	2	2254 (1681)	741.0
7	14	-59.98	0.095	32000	2	2219 (1655)	-494.0
7	14	-59.98	0.1	30316	2	2189 (1632)	-692.6

For the turbine, the three factors with the most impact on power delivered are inlet mass flow, inlet temperature and inlet pressure. Changing these parameters by roughly five percent lead to a power loss of 5.2, 7.1, and 8.0 percent, respectively.

All three of these quantities depend heavily on attributes of the rest of the engine (e.g., chamber combustion temperature, chamber length, materials of construction) and especially in the case of inlet pressure, on assumed performance characteristics (in this case, the pressure drop to be expected in the cooling jacket).

None of the factors evaluated on the pump side had as much impact on power requirement as the top three turbine factors. Pump power requirements were most affected by blade angle, blade thickness, and rotational speed. Among these parameters, rotational speed had the greatest impact. This parameter, in turn, is dependant on the turbine: in the absence of a gear box, both must rotate at the same speed.

Slowing the speed of the pump will necessitate a lower specific speed for the turbine and thus represents potential impact on turbine efficiency. While the speed in the Table 13 corresponds to a turbine specific speed of 0.415, still within the range suggested by Kofskey and Nusbaum[51] for maximum total efficiency, this parameter must be varied with care to avoid a deleterious impact on the turbine. Additionally, as pointed out in NASA SP-8107[11], throttling range usually increases with increasing specific speed for sweptback impellers with constant discharge blade angles due to the decrease in head coefficient with increasing specific speed. Therefore, a reduced pump speed is expected to result in a reduced throttling range.

4.4 Shaft and Bearings

The shaft diameter was determined based on stress criteria rather than stiffness (critical speed) criteria as is usual[54] since the rotodynamic analysis necessary to determine the latter quantity is outside the scope of this effort. From a stress perspective,

minimum required shaft diameter may be found by considering the power supplied by the turbine using the relations[55]:

$$\tau = \frac{P}{2\pi f} \tag{54}$$

$$\frac{J}{c} = \frac{\tau}{\sigma_{allowable}} \tag{55}$$

$$\sigma_{allowable} = \frac{\sigma_y}{\delta} \tag{56}$$

J is the polar moment of inertia, f is frequency (in Hz), c is the shaft radius, P is the turbine's power output, σ_y is the yield stress (found to be 168 ksi for Inconel 718[56]), $\sigma_{allowable}$ is the allowable stress, δ is a safety factor (chosen to be 1.2 in accordance with the safety factor chosen for the RL-10[54]) and τ is the shaft torque. The shaft must thus be at least 0.26 in (6.604mm) in diameter; this would correspond to a DN number of about 211,000. Based on the relatively low DN number and the need to meet IHPRPT's reliability and maintainability goals, a ceramic hybrid ball/hydrostatic bearing is the best choice for this application; these have been tested up to a DN number of 3 million[57]. The primary motivation for selecting these bearings is to take advantage of the long service life of hydrostatic bearings[26] while using ball bearings to accommodate the transient loads occurring at start-up and shut down. Ceramic balls are preferred due to their increased resistance to liquid oxygen relative to steel.

The maximum shaft length, which is calculated based on the maximum allowable deflection, is calculated from the relation given by Karassik, et al.[58]:

$$f = \frac{wl^3}{CEI} \tag{57}$$

where f is the shaft deflection (a maximum allowable value of 0.006 in (0.152 mm) was chosen), w is the weight of the rotating elements, C is a coefficient which depends on load distribution and shaft support method (set to one for purposes of this calculation), E is the modulus of elasticity, and I is the moment of inertia. For an Inconel 718 shaft, the maximum length is 3.4 in. The expected axial loads and fatigue limits calculated by the Concepts NERC software AxCENT[59] for Inconel-718 are shown in Table 14 and suggested bearing locations are shown in Figure 18. A representation of the final integrated rotor is found in Figure 19.

Table 13: Axial loads and fatigue limits

Net Force on Pump Impeller, lb_f (N)	195.8 (871)
Net Force on Turbine Rotor, lb_f (N)	-237.9 (1058)
Turbine Bore Stress level, ksi (MPa)	40.15 (276.8)
Pump Bore Stress level, ksi (MPa)	36.11 (249.0)
Turbine High Cycle Fatigue Margin at Design Speed, ksi (MPa)	57.88 (399.0)
Pump High Cycle Fatigue Margin at Design Speed, ksi (MPa)	69.82 (481.4)
Low Cycle Fatigue Limit at Design Speed	$> 10^6$ cycles

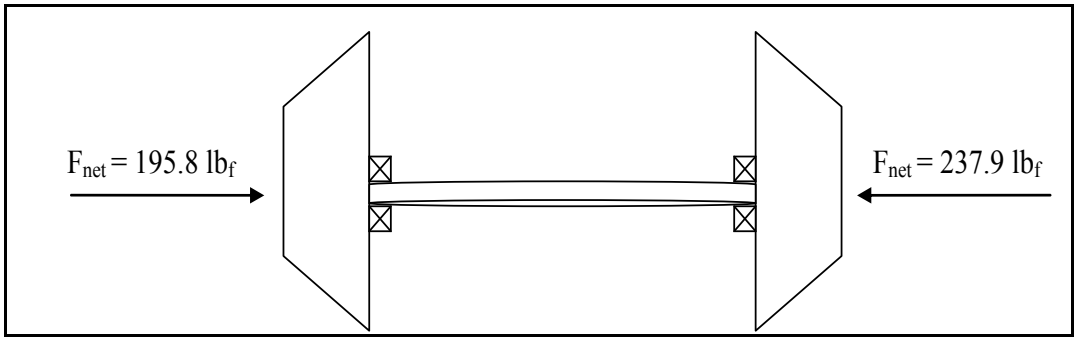

Figure 19: Bearing arrangement

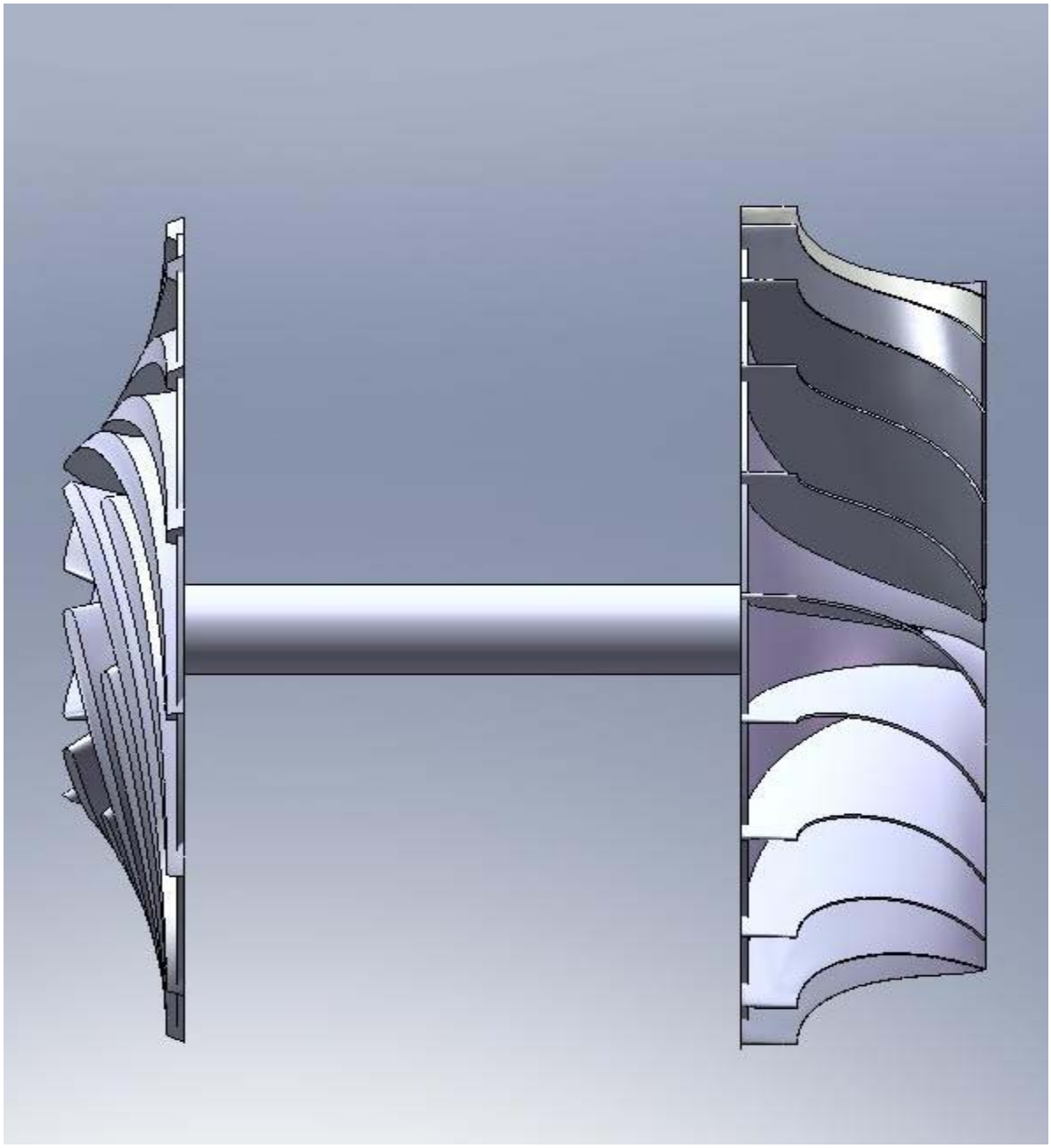

Figure 20: Final integrated rotor

5 Conclusions and Recommendations

This research effort was undertaken to examine the design of an oxygen pump to support a dual-expander engine concept (the DEAN) intended to meet the Phase III goals of the IHPRPT program. The main thrust of this program is to ensure reliable access to space and make space launch more efficient from both a monetary and time perspective. This effort used software that employs industry standard techniques and practices that satisfy governing equations and physics to model and predict pump and turbine performance. [38,44,59]

5.1 Conclusions

A LOX pump powered by warm gaseous oxygen is a plausible candidate for use in a dual expander cycle upper stage engine that will meet the performance, reliability, maintainability, and service life goals of IHPRPT Phase III.

Inconel 718 is the recommended material of construction for both the pump and the turbine due to its record of satisfactory service in oxygen and favorable mechanical properties, including its good ductility at cryogenic temperatures and high yield strength. Monel K-500, while exhibiting good oxygen resistance, does not possess the strength of Inconel 718. The expected turbine inlet temperature (600 R) is 55 percent of the ignition temperature of Inconel 600 demonstrated in Schoenman's friction rubbing test[24]. Additionally, Schoenman found that Monel, 400, 316 Stainless Steel, and Nickel 200 became more difficult to ignite and burn at oxygen pressures above 1000 psi (6.89 MPa)[23]; if this trend holds for Inconel then the difference in oxygen resistance may be insignificant at the pressures expected in the turbine. While Inconel 600 and Inconel

718 would be expected to behave similarly (based on their similar composition), a further test would be prudent.

The factors most affecting the turbine's power output are inlet temperature, inlet total pressure, and mass flow rate. These quantities are highly dependant on engine characteristics outside the pump designer's purview. Therefore, this system will be heavily influenced by engine design choices affecting chamber cooling.

The pump's power requirements are most affected by blade angle, blade thickness, and rotational speed, with the last having the most impact and being directly dependant on the turbine. While the pump appears to have ample NPSH, the addition of a small boost pump such as that used by Buckmann, et al.[10] or an axial inducer ahead of the impeller (such as those investigated by Kamijo et al.[60], Shimagaki, et al.[61], and Bramanti, Cervone, and d'Agostino[62]) is advisable.

The pump is capable of throttling down to 52 per cent of its maximum flow at design speed. While it may successfully operate at lower flow rates, it is likely the head rise at these lower flow rates will be insufficient to meet the engine's demands.

This study examined the design of an oxygen pump intended for use with a dual expander engine concept. This pump must be capable of supporting Phase III IHPRPT goals of maintainability, reliability, and supportability in addition to providing the flow and head rise demanded by the DEAN engine concept. The pump presented will provide ample flow at an appropriate pressure at the design point and will be capable of a wide throttling range. The turbine presented supplies adequate power over a wide range of desired flow rates. Its output is highly dependant on other engine characteristics, particularly the combustion chamber. The hydrostatic liftoff bearing will maximize the

likelihood of achieving the reliability, maintainability, and service life goals of the IHPRPT program.

5.2 Recommendations for Future Research

First, as this study focused on the hydrodynamic design of the pump and turbine, a rotodynamic analysis of the turbopump is in order.

Also, this study used a constant turbine nozzle loss coefficient based on a relation given by Dixon[41] for well-designed nozzle rows in normal operation and software package guidance[44]; a nozzle designed for this application with calculated losses would give more reliable results.

The turbine uses all full blades with no splitters. While Rohlik[63] suggests only a modest improvement is possible by replacing half the blades with splitters, it should be investigated.

Furthermore, while the turbine is operating in a favorable specific speed for attainment of high efficiency, the same may not be true of the pump. A trade study may find another rotational speed that achieves higher pump efficiency and perhaps a deeper throttling range while having a minimal effect on the turbine.[11]

Finally, a water/air flow test on a model of the pump and turbine would help to define performance and validate the design methods and loss models used. Conversely, it may show the need to use alternative loss models.

Appendix A

RITAL Inputs

Inlet Conditions

Total Temperature	600R
Total Pressure	3663psi
Mass Flow	95.0 lbm/s
Rotational Speed	32000 rpm

Nozzle Geometry

Inlet tip radius	3.40836 in
Inlet hub radius	3.40836 in
Inlet blade height	0.243 in
Exit tip radius	2.9 in
Exit hub radius	3.40836 in
Exit blade height	0.243044 in
Number of blades	15
Blade TE normal thickness	.035446 in
Vane Cord Length	0.5
Throat area multiplier	1.0

Nozzle Properties

Inlet blockage	0.02
Loss coefficient	0.0395
Trailing edge loss multiplier	0.2
Fraction of loss upstream of throat	0.3
Throat aerodynamic blockage	0.05

Nozzle Options

Loss model	User Specified Loss Coefficient
Deviation model	Modified Howell Correlation
Constants	a_3= 0.13

Interspace

Swirl coefficient	1.0
Inlet blockage	0.01
Loss coefficient	0.001

Rotor Geometry

Inlet:		Exit
Tip radius	2.8 in	2.3 in
Hub radius	2.8 in	0.75 in
Blade height	0.35 in	
Blade angle	0.0 degrees	-60 degrees
Blade TE normal thickness		0.03 in

Rotor throat area multiplier	1.0
Number of blades	22
Suction Surface blade thickness at throat	0.05 in
Axial clearance	0.0035 in
Radial clearance	0.007724 in
Back face clearance	0.0035 in

Rotor Properties

Optimum incidence	-35.0 degrees
Inlet blockage	0.1
Rotor throat aerodynamic blockage	0.05
Rotor exit deviation	3.0 degrees
Trailing edge loss multiplier	1.0
Fraction of loss upstream of throat	0.6
Rotor loss model	NASA passage loss

Rotor Loss Coefficient Multipliers

Incidence	1.0
Passage	0.1
Axial clearance	0.4
Radial clearance	0.75

Exit Conditions

Blockage	0.0
Exit total pressure	2035

PUMPAL Inputs

Upstream Conditions

Stagnation temperature	150 R
Stagnation pressure	45 psi
Rotational Speed	32000 rpm

Impeller Inlet-Geometry

Dimensions	Variable
Hub radius	0.760267
Setback angle	36.9 degrees
Number of main blades	7
Leading edge thickness	.0625
Incidence (Tip, hub, and RMS)	2 degrees

Impeller Inlet-Properties

Blockage	0.083337
Velocity Ratio	1.05
LC1	0.01
Flow angle correction	0.0

Impeller Inlet-Options	
Inlet incidence (hub,mean, and tip)	Input
Inducer optimization	For Min. NPSHR
LC1	Constant
Swirl Option	Set s. angle directly
Impeller Exit-Geometry	
Rotor Design Option	Optimize R2 and B2
PHI2	90.0 degrees
BEATA2B, Mean	-59.98
Number of exit blades	14
Blade thickness	0.1 in
Bexp ratio	1.0
Impeller Exit-Properties	
Msec/M	0.550682
DELTAs	0.0
DELp option	Nominal
LAM2	4.2
DF multiplier	1.0
Design Target	Pressure
Pressure Rise Multiplier (safety factor)	1.02
ETAa:	0.0
ETAb	0.0

Impeller Exit-Options	
Impeller tip model	Two-zone: Frozen
Slip model	Preferred deviation function
Slip definition	American
Disk friction	Rear disk friction only
Recirculation power	Variable Power
Impeller Diffusion	Specific Speed Function
Two-zone calculation	Based on tip to tip
Exit width design model	User Specified Lam2
Volute-Geometry	
Dimensions	Variable
Type	Symmetric (22.5 deg)
Nominal Area at 0 degrees	Fixed
Radius (VR7/R5)	1.0
Station 8 exit diameter ratio	2.0
Volute-Properties	
LC57Mult	1.0
CP57	-1.370E-4
CP78Mult	1.0
Volute exit cone model	Blockage correction
Impeller exit area multiplier	1.1

Bibliography

[1] M. Blair and D. DeGeorge, "Overview of the Integrated High Payoff Rocket Propulsion Technology Program", IAF-00-S.3.07, *51st International Astronautical Congress*, Rio de Janerio, Brazil October 2000.

[2] London, John R., *LEO On The Cheap*, Maxwell Air Force Base, AL: Air University Press, October 1994.

[3] Stucke, Brian A. and Anderl, Timothy R. , "Doubling our Reach to Space," *The AMPTIAC Quarterly*, Volume 8, Number 1, 2004, pp.35-38.

[4] Michael D. Berglund, Dan Marin, and Mark Wilkins, *The Next-Generation Heavy-Lift Vehicle— The Inaugural Flight of the EELV Delta IV Heavy*, AIAA 2005-6707.

[5] Sweetman, Bill, ed. *Jane's Space Directory 2006-2007*, p.270; Alexandria, VA : Jane's Information Group, 2006.

[6] Alliot, P., Dalbies, E, Delange, J-F, and Ruault, J-M, *Development status of the VINCI engine for the Ariane 5 upper stage* AIAA 2003-4484.

[7] Dieter K. Huzel and David H. Huang, *Modern Engineering for Design of Liquid-Propellant Rocket Engines*, Washington: American Institute of Aeronautics and Astronautics, Inc., 1992.

[8] Sweetman, Bill, ed. *Jane's Space Directory 2006-2007*, pp. 360-361; Alexandria, VA : Jane's Information Group, 2006.

[9] P.S. Buckmann, N.R. Shrimp, F. Viteri, and M. Proctor, "Design and Test of an Oxygen Turbopump for a Dual Expander Cycle Rocket Engine," *Journal of Propulsion and Power*, Vol. 8, no. 1, Jan-Feb 1992, pp. 80-86.

[10] P.S. Buckmann, W.R. Hayden, S.A. Lorenc, R.L. Sabiers, and N.R. Shrimp, *Orbital Transfer Vehicle Oxygen Turbopump Technology: Final Report, Volume 1- Design, Fabrication, and Hydrostatic Bearing Testing*, NASA CR-185175, December 1990.

[11] National Aeronautics and Space Administration, *Turbopump Systems for Liquid Rocket Engines*, NASA SP-8107, August 1974

[12] Sutton, George P., *Turbopumps, a Historical Perspective*, AIAA-2006-5033.

[13] Binder, M.P. *A Transient Model of the RL10A-3-3A Rocket Engine*, AIAA-95-2968.

[14] R.J. Brannam, P. S Buckmann, B. H. Chen, S. J. Church, and R. L Sabiers, *Orbital Transfer Vehicle Oxygen Turbopump Technology: Final Report, Volume 2- Nitrogen and Ambient Oxygen Testing*, NASA CR-185262, December 1990.

[15] Masumi Fujita and Yukio Fukushima, *Improvement of LE-5A and LE-7 Engine,* AIAA 96-2847, July 1996.

[16] Ronny Johnsson, Staffan Brodin, Per Ekedahl, Lennard Helmers and Johan Hogstrom, *Development of Hydrogen and Oxygen Pump Turbines for Vinci Engine*, AIAA 2002-4331.

[17] Urke, Robert L. , *Orbital Transfer Vehicle Oxygen Turbopump Technology: Final Report, Volume 3-Hot Oxygen Testing*, NASA CR-191036.

[18] National Aeronautics and Space Administration, *Liquid Rocket Engine Centrifugal Flow Turbopumps*, NASA SP-8109, December 1973.

[19] Campbell, W.E and Farquhar, J. "Centrifugal Pumps for Rocket Engines" in *Fluid Mechanics, Acoustics, and Design of Turbomachinery, Part II* NASA SP-304, Washington: National Aeronautics and Space Administration, 1974.

[20] Fukushima, Y and Imoto, T, *Lessons Learned in the Development of the LE-5 and LE-7* AIAA-94-3375.

[21] Barton, John, et al, *Cryogenic Engines in Western Europe: From Exploratory Developments to Vulcain and Vinci*, AIAA 99-2904.

[22] National Aeronautics and Space Administration *Liquid Rocket Engine Turbines*, NASA SP-8110, January 1974.

[23] Schoenman, Len, "Selection of Burn-Resistant Materials for Oxygen-Driven Turbopumps", *Journal of Propulsion and Power*, Vol. 3, no.1, pp.46-55, Jan-Feb 1987.

[24] Schoenman, Leonard. *Orbital Transfer Rocket Engine Technology Program Final Report: Oxygen Materials Compatablility Testing,* NASA CR-182195. January 1989 .

[25] Mohr, David "Turbomachines in Rocket Propulsion Systems," in *Handbook of Turbomachinery* , 2nd edition, Ed. Earl Logan and Ramendra Roy. New York: Marcel Dekker, Inc. 2003.

[26] Scharrer, Joseph, Hibbs, Robert I., Nolan, Steven A., and Tabibzadeh, Ramin, *Extending the Life of the SSME HPOTP Through the Use of Annular Hydrostatic Bearings*, AIAA-92-3401.

[27] Scharrer, J.K., Tellier, J.G., and Hibbs, R.I., *Start Transient Testing of an Annular Hydrostatic Bearing in Liquid Oxygen*, AIAA 92-3404.

[28] Meyer, Lee, Nichols, James, Krach, Ann, and LeClaire, Richard, *Next Generation of Reuseable Launch Vehicle Engines: Current Technologies that Support Next Generation Engines*, AIAA 95-3156.

[29] Humble, Ronald W., Henry, Gary N., and Larson, Wiley J. *Space Propulsion Analysis and Design*. New York: McGraw-Hill, 1995.

[30] Wilson, David Gordon and Korakianitis, Theodosios, *The Design of High-Efficiency Turbomachinery and Gas Turbines*, 2nd ed., Upper Saddle River, NJ: Prentice-Hall, 1998.

[31] National Aeronautics and Space Administration,*Turbine Design and Application*, Arthur J. Glassman, Ed. NASA SP-290, Washington: National Aeronautics and Space Administration, 1994.

[32] Oyama, Akira and Liou, Meng-Sing, "Multiobjective Optimization of Rocket Engine Pumps Using Evolutionary Algorithm", *Journal of Propulsion and Power*, Vol. 18, no.3, May-June 2002, pp. 528-535.

[33] Veres, Joseph P. *Centrifugal and Axial Pump Design and Off-Design Performance Prediction*, NASA TM-106745, October 1994.

[34] Veres, Joseph P., *A Survey of Instabilities Within Centrifugal Pumps and Concepts for Improving the Flow Range of Pumps in Rocket Engines*", NASA TM-105439.

[35] Rohlik, Harold E., "Radial Inflow Turbines", in *Turbine Design and Application*, Arthur L. Glassman, ed. NASA SP-290, Washington: National Aeronautics and Space Administration, 1994.

[36] Dixon, S.L., *Fluid Mechanics and Thermodynamics of Turbomachinery*, 4th ed., Boston: Butterworth-Heinemann, 1998.

[37] National Aeronautics and Space Administration, Numerical Propulsion Simulation System, v1.6.4, 30 May 2006

[38] *Pumpal*. Version 7.9.30. Computer Software. Concepts NERC, White River Junction, VT, 2006.

[39] Japikse, David, Marscher, William D., Furst, Raymond B., *Centrifugal Pump Design and Performance*, White River Junction, VT: Concepts ETI, Inc., 2006.

[40] Concepts NERC, *PUMPAL HELP*, White River Junction, VT, 2006.

[41] Dixon, S.L., *Fluid Mechanics and Thermodynamics of Turbomachinery*, 4th ed., Boston: Butterworth-Heinemann, 1998 .

[42] Aungier, Ronald H., *Turbine Aerodynamics- Axial-Flow and Radial-Inflow Turbine Design and Analysis*, New York: ASME Press, 2006

[43] NIST Webbook, http://webbook.nist.gov/chemistry/fluid/

[44] *Rital*. Verison7.11.2.0. Computer Software. Concepts NERC, White River Junction, VT, 2006.

[45] Moustapha, Hany, Zelesky, Mark F., Baines, Nicholas C. and Japikse, David, *Axial and Radial Turbines*, Concepts ETI, Inc. 2003.

[46] Concepts NERC, *RITAL HELP* White River Junction, VT, 2006.

[47] Mathis, David M., "Fundamentals of Turbine Design" in *Handbook of Turbomachinery, 2nd Ed.*, Earl Logan and Ramendra P. Roy, Eds. , Marcel Dekker, Inc. New York 2003

[48] Futral, Samuel M. Jr, and Holeski, Donald E., *Experimental Results of Varying the Blade-Shroud Clearance in a 6.02-Inch Radial-Inflow Turbine*, NASA TN D-5513, 1970.

[49] Jansen, W, "The Design and Performance Analysis of Radial-Inflow Turbines", NREC report 1067-1.

[50] Perry, Robert, Green, Don W., and Maloney, James O., eds. *Perry's Chemical Engineer's Handbook*, 7th ed., New York: McGraw-Hill, 1997.

[51] Kofskey, Milton and Nusbaum, William, *Effects Of Specific Speed On Experimental Performance Of A Radial Inflow Turbine*, NASA TND-6605, 1972.

[52] Kofskey, Milton and Holeski, Donald, *Cold performance evaluation of a 6.02-inch radial inflow turbine designed for a 10-kilowatt shaft output Brayton cycle space power generation system*, NASA TND-2987, 1966.

[53] Milton G. Kofskey and Charles A. Wasserbauer. *Experimental evaluation of a 3.50-inch radial turbine designed for a 10-kilowatt space power system,* NASA TN-D5550, 1969.

[54] National Aeronautics and Space Administration ,*Liquid Rocket Engine Turbopump Shafts and Couplings*, NASA SP-8101, September 1972.

[55] Beer,Ferdinand, and Johnson, E. Russell, *Mechanics of Materials*, 2nd ed., New York: McGraw-Hill, 1981.

[56] Kutz, Meyer, ed. *Mechanical Engineer's Handbook*, New York: John Wiley and Sons, 1998.

[57] Ohta,T, Kimoto, K., Kawai,T., and Motomura,T., *Design, Fabrication, and Test of the RL60 Fuel Turbopump*, AIAA 2003-5073, July 2003.

[58] Karassik, Igor, Messina, Joseph P., Cooper, Paul, and Heald, Charles C., Ed., *Pump Handbook,*3rd ed., New York: McGraw-Hill, 2001.

[59] Concepts NERC, AxCent v. 7.9.16.0, July 2006.

[60] Kenjiro Kamijo, Hitoshi Yamada, Norio Sakazume and Shogo Warashina, "*Developmental History of Liquid Oxygen Turbopumps for the LE-7 Engine*", Trans. Japan Soc. Aero. Space Sci., Vol. 44, No. 145, pp. 155–163, 2001.

[61] Mitsuru Shimagaki, Toshiya Kimura, Tomoyuki Hashimoto, Mitsuo Watanabe, and Yoshiki Yoshida, *Investigation of Backflow Structure in a Turbopump Inducer with the PIV Method*, AIAA 2007-5512.

[62] Cristina Bramanti, Angelo Cervone, and Luca d'Agostino, *A Simplified Analytical Model for Evaluating the Noncavitating Performance of Axial Inducers*, AIAA 2007-5514.

[63] Rohlik, Harold E., Analytical Determination of Radial Inflow Turbine Design Geometry for Maximum Efficiency, NASA-TN D-4384, February 1968.

Vita

Capt William Strain graduated from Colorado Springs Christian School, Colorado Springs, CO in 1995. He attended Columbia University, New York, NY and graduated with a Bachelor of Science in Chemical Engineering in 1999. After working in the pharmaceutical and oilfield service industries, he attended Officers' Training School at Maxwell AFB, AL and received his commission in the United States Air Force in 2003.

Capt Strain's first assignment was to Kirtland AFB, NM where he was a Laser System Engineer in the Airborne Laser System Program Office. He entered the Graduate School of Engineering and Management, Air Force Institute of Technology, WPAFB, Ohio in March 2006. After graduation, he will be assigned to the National Air and Space Intelligence Center, WPAFB, OH.

REPORT DOCUMENTATION PAGE

Form Approved
OMB No. 074-0188

1. REPORT DATE *(DD-MM-YYYY)*	**2. REPORT TYPE**	**3. DATES COVERED** *(From – To)*
27-03-2008	Master's Thesis	March 2006 – March 2008

4. TITLE AND SUBTITLE

Design Of An Oxygen Turbopump For A Dual Expander Cycle Rocket Engine

5a. CONTRACT NUMBER

5b. GRANT NUMBER

5c. PROGRAM ELEMENT NUMBER

6. AUTHOR(S)

Strain, William S., Captain, USAF

5d. PROJECT NUMBER

5e. TASK NUMBER

5f. WORK UNIT NUMBER

7. PERFORMING ORGANIZATION NAMES(S) AND ADDRESS(S)

Air Force Institute of Technology
Graduate School of Engineering and Management (AFIT/EN)
2950 Hobson Way, Building 640
WPAFB OH 45433-8865

8. PERFORMING ORGANIZATION REPORT NUMBER

AFIT/GAE/ENY/08-M26

9. SPONSORING/MONITORING AGENCY NAME(S) AND ADDRESS(ES)

Mr. Michael Huggins
AFRL/PRS
5 Pollux Dr., Edwards AFB, CA 93524-7680

10. SPONSOR/MONITOR'S ACRONYM(S)

11. SPONSOR/MONITOR'S REPORT NUMBER(S)

12. DISTRIBUTION/AVAILABILITY STATEMENT

APPROVED FOR PUBLIC RELEASE; DISTRIBUTION UNLIMITED.

13. SUPPLEMENTARY NOTES

14. ABSTRACT

The design of a pump intended for use with a dual expander cycle (LOX/H_2) engine is presented. This arrangement offers a number of advantages over hydrogen expander cycles; among these are the elimination of gearboxes and inter-propellant purges and seals, an extended throttling range, and higher engine operating pressures and performance. The target engine has been designed to meet the needs of Phase III of the Integrated High Payoff Rocket Propulsion Technology (IHPRPT) program; thus, this pump must meet the program's reliability, maintainability, and service life goals. In addition, this pump will be driven by warm gaseous oxygen. In order to meet the needs of this engine, the pump will need to be capable of delivering 106 lbm/s (48.1 kg/s) at 4500 psi (31 MPa); this will necessitate a turbine capable of supplying at least 2215 hp (1652 kW). The pump and turbine were designed with the aid of an industry standard design program; the design methodology and justification for design choices are presented. Appropriate materials of construction and bearings for this pump are discussed.

15. SUBJECT TERMS

Dual expander cycle engine, LOX/H2, upper stage, turbopump, liquid oxygen, oxygen driven turbine, throttleability, NPSS, IHPRPT, hybrid bearings

16. SECURITY CLASSIFICATION OF:			**17. LIMITATION OF ABSTRACT**	**18. NUMBER OF PAGES**	**19a. NAME OF RESPONSIBLE PERSON**
a. REPORT	**b. ABSTRACT**	**c. THIS PAGE**			Richard D. Branam, Maj, USAF
U	**U**	**U**	**UU**	84	**19b. TELEPHONE NUMBER** *(Include area code)* (937) 255-3636, ext 7485 (rbranam@afit.edu)

Standard Form 298 (Rev. 8-98)
Prescribed by ANSI Std. Z39-18